Contact
Volume 7: 1–17
© The Author(s) 2024
Article reuse guidelines:
sagepub.com/journals-permissions
DOI: 10.1177/25152564241229273
journals.sagepub.com/home/ctc
Sage

Supralinear Dependence of the IP_3 Receptor-to-Mitochondria Local Ca^{2+} Transfer on the Endoplasmic Reticulum Ca^{2+} Loading

György Csordás[1], David Weaver[1], Péter Várnai[2], and György Hajnóczky[1]

Abstract

Calcium signal propagation from endoplasmic reticulum (ER) to mitochondria regulates a multitude of mitochondrial and cell functions, including oxidative ATP production and cell fate decisions. Ca^{2+} transfer is optimal at the ER-mitochondrial contacts, where inositol 1,4,5-trisphosphate (IP_3) receptors (IP3R) can locally expose the mitochondrial Ca^{2+} uniporter (mtCU) to high [Ca^{2+}] nanodomains. The Ca^{2+} loading state of the ER (Ca^{2+}_{ER}) can vary broadly in physiological and pathological scenarios, however, the correlation between Ca^{2+}_{ER} and the local Ca^{2+} transfer is unclear. Here, we studied IP_3-induced Ca^{2+} transfer to mitochondria at different Ca^{2+}_{ER} in intact and permeabilized RBL-2H3 cells via fluorescence measurements of cytoplasmic [Ca^{2+}] ($[Ca^{2+}]_c$) and mitochondrial matrix [Ca^{2+}] ($[Ca^{2+}]_m$). Preincubation of intact cells in high versus low extracellular [Ca^{2+}] caused disproportionally greater increase in $[Ca^{2+}]_m$ than $[Ca^{2+}]_c$ responses to IP_3-mobilizing agonist. Increasing Ca^{2+}_{ER} by small Ca^{2+} boluses in suspensions of permeabilized cells supralinearly enhanced the mitochondrial Ca^{2+} uptake from IP_3-induced Ca^{2+} release. The IP_3-induced local [Ca^{2+}] spikes exposing the mitochondrial surface measured using a genetically targeted sensor appeared to linearly correlate with Ca^{2+}_{ER}, indicating that amplification happened in the mitochondria. Indeed, overexpression of an EF-hand deficient mutant of the mtCU gatekeeper MICU1 reduced the cooperativity of mitochondrial Ca^{2+} uptake. Interestingly, the IP_3-induced $[Ca^{2+}]_m$ signal plateaued at high Ca^{2+}_{ER}, indicating activation of a matrix Ca^{2+} binding/chelating species. Mitochondria thus seem to maintain a "working $[Ca^{2+}]_m$ range" via a low-affinity and high-capacity buffer species, and the ER loading steeply enhances the IP3R-linked $[Ca^{2+}]_m$ signals in this working range.

Keywords

ER, mitochondria, calcium, uniporter, cooperativity, calcium buffering

Introduction

Ca^{2+} signals generated by IP_3 receptor (IP3R)-mediated Ca^{2+} mobilization from the ER can propagate to the mitochondrial matrix as $[Ca^{2+}]_m$ signals that activate matrix dehydrogenases and enhance ATP production (Denton et al., 1980; Hansford, 1987; Hajnoczky et al., 1995; Robb-Gaspers et al., 1998; Jouaville et al., 1999) but can also lead to Ca^{2+} overload and permeability transition pore (mPTP) activation to trigger cell injury or death (Szalai et al., 1999; Pinton et al., 2008). Although mitochondrial Ca^{2+} uptake generally shows little activation at <1 μM $[Ca^{2+}]_c$ levels (Gunter and Pfeiffer, 1990; Kirichok et al., 2004), IP3R-linked $[Ca^{2+}]_c$ spikes and oscillations in this range can effectively evoke rapid increases in $[Ca^{2+}]_m$ (Rizzuto et al., 1992). This paradox has been explained by a local Ca^{2+} delivery between closely apposed segments of ER and mitochondria where IP3R-mediated Ca^{2+} release can expose the mitochondrial surface to 10–30 μM [Ca^{2+}] (Rizzuto et al., 1998; Csordas et al., 1999, 2010; Giacomello et al., 2010). Mitochondria can also exert local control over $[Ca^{2+}]_c$ signals by a number of mechanisms: directly via mitochondrial Ca^{2+} uptake (Szabadkai and Duchen, 2008), indirectly by funneling Ca^{2+} from store-operated entry channels to the SERCA pumps (Malli

[1]MitoCare Center for Mitochondrial Imaging Research and Diagnostics, Department of Pathology, Anatomy and Cell Biology, Thomas Jefferson University, Philadelphia, PA, USA
[2]Department of Physiology, Semmelweis Medical University, Budapest, Hungary

Received December 4, 2022; Revised December 31, 2023; Accepted January 12, 2024

Corresponding Authors:
György Csordás, MitoCare Center for Mitochondrial Imaging Research and Diagnostics, Department of Pathology, Anatomy and Cell Biology, Thomas Jefferson University, Philadelphia, PA, USA.
Email: Gyorgy.Csordas@jefferson.edu

György Hajnóczky, MitoCare Center for Mitochondrial Imaging Research and Diagnostics, Department of Pathology, Anatomy and Cell Biology, Thomas Jefferson University, Philadelphia, PA, USA.
E-mail: gyorgy.hajnoczky@jefferson.edu

et al., 2003), by energy supply (Jouaville et al., 1995), or by redox modulation of IP3Rs (Booth et al., 2016; Booth et al., 2021). Local Ca^{2+} clearance by mitochondria also contributes to the shaping of $[Ca^{2+}]_c$ by relieving feedback inhibition of the IP3Rs as well as the store-operated Ca^{2+} entry (SOCE) channels by Ca^{2+} (Hoth et al., 1997; Hajnoczky et al., 1999; Tinel et al., 1999; Marchant et al., 2002; Olson et al., 2010).

The fraction of Ca^{2+} delivered to the mitochondria during IP3R-mediated release can be substantial—at least in some cell types—up to ~30% in H9c2 and ~50% in RBL-2H3 cells (Pacher et al., 2000). The Ca^{2+} loading state of the ER determines the $[Ca^{2+}]$ gradient across the ER membrane and might modulate the local Ca^{2+} delivery from the IP3R to the mitochondria. $[Ca^{2+}]$ in the ER lumen ($[Ca^{2+}]_{ER}$) has also been linked to regulation of IP3R gating (Missiaen et al., 1992; Oldershaw and Taylor, 1993; Horne and Meyer, 1995; Vais et al., 2012, 2020). Furthermore, accumulating evidence suggests a positive correlation between Ca^{2+}_{ER} and mitochondrial apoptosis, which can be triggered by IP3R-derived Ca^{2+} transfer to the mitochondria (Szalai et al., 1999). Excessive ER loading upon SERCA2a overexpression has been shown to promote apoptosis in Cos-7 cells (Ma et al., 1999). On the other hand, decreased ER Ca^{2+} levels associated with ER-targeted overexpression of Bcl-2 attenuated IP3R-linked $[Ca^{2+}]_c$ and $[Ca^{2+}]_m$ signals and were protective against ceramide-induced apoptosis (Foyouzi-Youssefi et al., 2000; Pinton et al., 2000, 2001). Similarly, impaired ER Ca^{2+} accumulation in Bax/Bak double-knockout MEF cells caused 50%–60% reduction of agonist-induced $[Ca^{2+}]_c$ signals and almost completely eliminated $[Ca^{2+}]_m$ signals (Scorrano et al., 2003). Thus, a complex positive correlation is likely to exist between ER Ca^{2+} storage and IP3R-mediated Ca^{2+} transfer to the mitochondria, which has relevance for cell survival. Our goal was to quantitatively measure the amounts of Ca^{2+} locally transported to the mitochondria at the ER-mitochondrial contacts during IP3R activation. While fluctuations in the $[Ca^{2+}]_{ER}$ and $[Ca^{2+}]_m$ have been reported in previous studies (a nice example is Suzuki et al., 2014), these measurements could not address Ca^{2+} transfer relative to total ER Ca^{2+} content (Ca^{2+}_{ER}, please note the difference between Ca^{2+}_{ER} and $[Ca^{2+}]_{ER}$, the latter refers to the luminal $[Ca^{2+}]$ in the ER) because of the different Ca^{2+} binding species in each compartment and because of the limitations of fluorescent protein-based sensors, for example, environment sensitivity. Here we quantitatively characterize this relationship in RBL-2H3 cells, a cell model with highly efficient local IP3R-to mitochondria Ca^{2+} delivery.

Results

IP_3-Linked $[Ca^{2+}]_c$ Signals Propagate to the Mitochondria More Effectively With Increasing ER Ca^{2+} Loading

First, we tested the effect of changes in the Ca^{2+} loading state of the ER on the efficacy of IP_3-linked $[Ca^{2+}]_c$ signal propagation to the mitochondrial matrix. To establish low and high ER Ca^{2+} loading state (Ca^{2+}_{ER}), intact RBL-2H3 cells were preincubated in an extracellular medium (ECM), from which the $CaCl_2$ was either omitted (Figure 1A "low," $[Ca^{2+}]_{EC}$ ~1 μM) or increased to 10 mM (from the normal 2 mM) (Figure 1A "high"), respectively. To minimize the contribution of SOCE, the agonist-induced $[Ca^{2+}]_c$ (fura-2/AM) and $[Ca^{2+}]_m$ (mtpericam) responses were recorded without added $CaCl_2$ in the ECM in both conditions ($[Ca^{2+}]_{EC}$ ~1 μM). Preincubation in high $[Ca^{2+}]_{EC}$ slightly elevated the resting $[Ca^{2+}]_c$ ($[Ca^{2+}]_c$ 70 ± 1.4 nM vs. 50 ± 2.5 nM, $N = 3$ experiments, 2-3 coverslips each, $p = .031$) but not $[Ca^{2+}]_m$ (Figure 1D), indicating that the pretreatment could feed the high-affinity ER Ca^{2+} pumps (SERCA) without enhancing mitochondrial Ca^{2+} uptake in unstimulated cells. To activate the IP3Rs, muscarinic m1 receptors were transiently overexpressed and stimulated by a supramaximal dose of carbachol (CCh, 100 μM). The CCh-stimulated $[Ca^{2+}]_c$ spike was ~33% larger (peak magnitudes 630 ± 125 nM vs. 475 ± 130 nM, $N = 3$; $p < .01$ with paired *t*-test) and more sustained in the cells preincubated in high $[Ca^{2+}]_{EC}$, consistent with a greater Ca^{2+} release from the better loaded ER (Figure 1B and C, green). The associated rapid and sustained $[Ca^{2+}]_m$ elevation was disproportionally (twice on average) larger in the cells preincubated in high $[Ca^{2+}]_{EC}$ ECM as compared to those in low $[Ca^{2+}]_{EC}$ buffer (Figure 1B and C, magenta). This difference was consistently observed using two different mitochondrial matrix-targeted Ca^{2+} probes (ratiometric and inverse pericam, Figure1 C). The rapid upstroke phase comprised ≥80% of the CCh-stimulated $[Ca^{2+}]_m$ rise, and it generally ended by the time the $[Ca^{2+}]_c$ spike reached its peak (in ~4 s), which is the point when ER release flux is overcome by cytosolic Ca^{2+} clearance pathways. Thus, the bulk of the $[Ca^{2+}]_m$ signal originated from mitochondrial Ca^{2+} uptake during the peak period of ER Ca^{2+} release, when the mitochondrial uptake sites were presumably exposed to the short-lasting, IP3R-mediated high $[Ca^{2+}]_c$ nanodomains. Of note, we couldn't completely rule out a contribution of SOCE in the sustained phase of the $[Ca^{2+}]$ responses because some Ca^{2+} entry can occur even at $[Ca^{2+}]_{EC}$ ~1 μM but SOCE cannot account for the differences in the $[Ca^{2+}]_c$ and $[Ca^{2+}]_m$ signals obtained at different Ca^{2+} preloads because the stimulation was performed at the same $[Ca^{2+}]_{EC}$ ~1 μM in each condition. Furthermore, mitochondrial Ca^{2+} uptake was not suppressed in the cells preincubated in low $[Ca^{2+}]_{EC}$, since exposure to SOCE following the Cch stimulation could elevate $[Ca^{2+}]_m$ to similar levels as in the cells preincubated in high $[Ca^{2+}]_{EC}$ (Figure 1B, magenta). The minimal further $[Ca^{2+}]_m$ increase upon SOCE in the high $[Ca^{2+}]_{EC}$ preincubation condition might be due to saturation of Ca^{2+}. These results suggest a steeper dependence of the IP3R-linked $[Ca^{2+}]_m$ signals than the $[Ca^{2+}]_c$ signals on Ca^{2+}_{ER}.

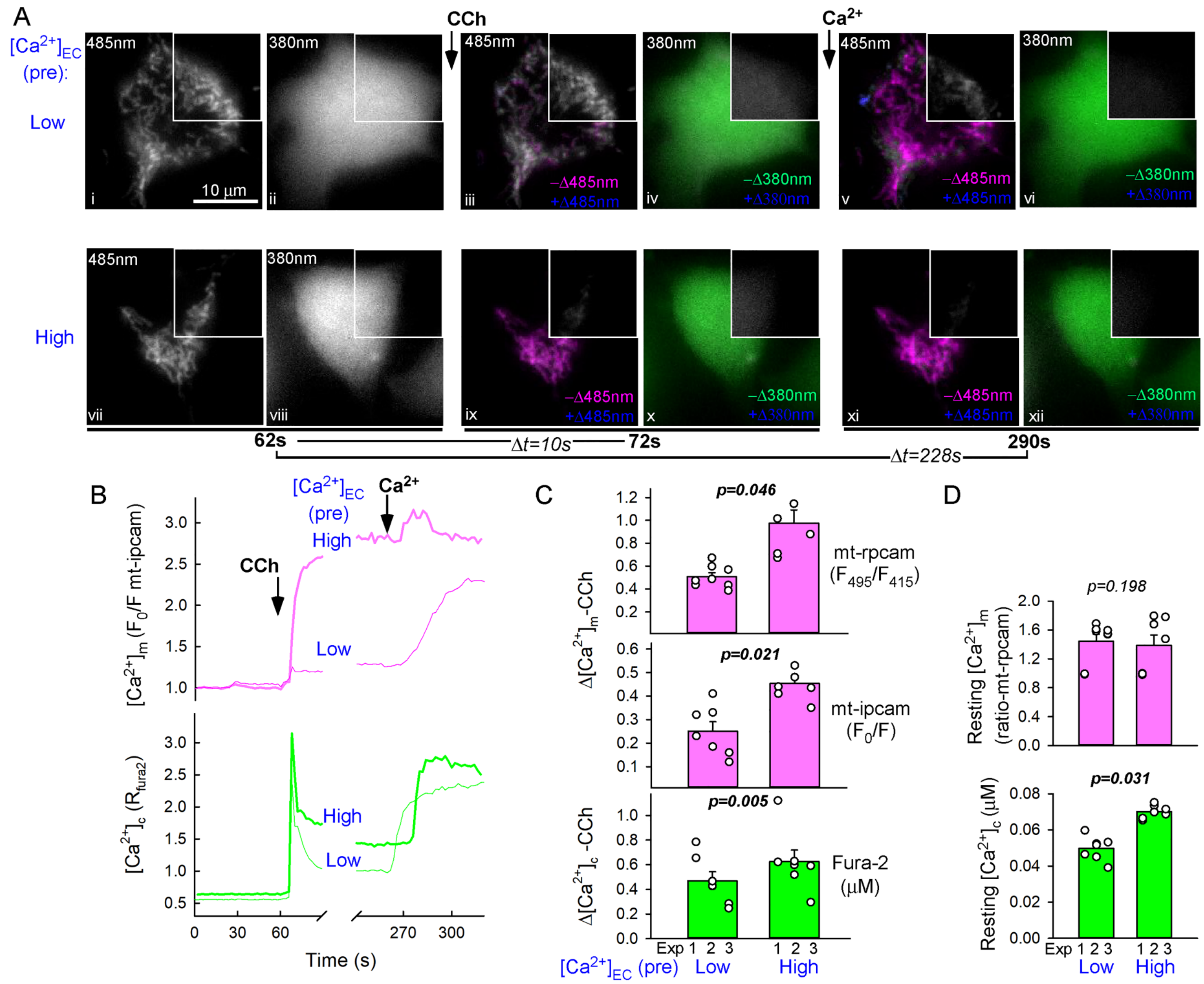

Figure 1. Ca^{2+} Loading of the ER Promotes IP_3-Linked Ca^{2+} Signal Transmission to the Mitochondria in Intact RBL-2H3 Cells.
ER Ca^{2+} loading was manipulated by preincubating the cells in extracellular buffer with no added Ca^{2+} (low, $[Ca^{2+}]_{EC}$ ∼1 μM) or containing 10 mM $CaCl_2$ (high) for 30 min. Just before the recordings all samples were washed into nominally Ca^{2+}-free buffer ($[Ca^{2+}]_{EC}$ ∼1 μM). $[Ca^{2+}]_c$ and $[Ca^{2+}]_m$ responses evoked by carbachol (CCh 100 nM) were either simultaneously recorded as the fluorescence of fura-2 (340/380 nm excitation) and inverse pericam (mt-ipcam, 495 nm excitation), respectively or, since inverse pericam in some cases displayed saturation upon high-Ca^{2+} pretreatment, $[Ca^{2+}]_m$ responses were also tested using ratiometric pericam (mt-rpcam) in separate recordings (C, top). As a reference, in the end of each run, physiological $[Ca^{2+}]_{EC}$ was restored by addition of 2 mM $CaCl_2$ (Ca^{2+}), evoking robust SOCE. (A) high-resolution time series images of exemplar RBL-2H3 cells preincubated in low (upper, i-vi) and high (lower, vii-xii) $[Ca^{2+}]_{EC}$. The horizontal image pairs (3 each) show the fluorescence on 16-bit grayscale for the mt-ipcam (odd numbers) and corresponding cytoplasmic fura-2 @380 nm excitation (even numbers) at rest (@62 s, the time of CCh addition, i-ii & vii-viii), 10 s post CCh stimulation (@72 s, ii-iv & ix-x) and 30 s post Ca^{2+} back-addition (@290 s, v-vi & xi-xii). The post-stimulation images (iii-vi & ix-xii) are overlaid with the corresponding difference (>300 intensity units) images depicting the decreases (ipericam purple, fura-2 green pseudocolors) and increases (blue pseudocolors) in fluorescence. Upper right quadrants (white frames) show the grayscale fluorescence without overlay. (B) Time courses of $[Ca^{2+}]_c$ and $[Ca^{2+}]_m$ recorded from the cells in (A). (C) Amplitudes of $[Ca^{2+}]_c$ and $[Ca^{2+}]_m$ (both, mt-ipcam and mt-rpcam) responses to CCh stimulation in cells pretreated in high/low Ca^{2+} buffer. (D) Resting $[Ca^{2+}]_c$ (fura-2, translated to μM) and $[Ca^{2+}]_m$ (mt-rpcam ratio) levels in the two conditions. Means ±S.E. from three experiments (data points for the individual experiments are indexed as Exp 1, 2, 3 at the bottom).

$[Ca^{2+}]_m$ Signals Associated With IP_3-Stimulated Ca^{2+} Release in Permeabilized Cells Steeply Depend on ER Ca^{2+} Loading State

Quantitative assessment of the IP3R-mediated Ca^{2+} transfer to the mitochondria as a function of ER Ca^{2+} storage is not feasible in intact cells because no approach has been set up to dynamically monitor the amount of Ca^{2+} in the relevant compartments. To further investigate the dependence of $[Ca^{2+}]_m$ on Ca^{2+}_{ER}, we used suspensions of permeabilized cells, which model $[Ca^{2+}]$ in the ($[Ca^{2+}]_{bm}$) as a proxy for $[Ca^{2+}]_c$ that can be directly manipulated and its Ca^{2+}

content quantified. This then gives the opportunity to quantify the Ca^{2+} sequestered by or released from the ER and/or mitochondria. In gently permeabilized RBL-2H3 cells, many aspects of possible organelle damage have been excluded and the ER-mitochondrial local Ca^{2+} transfer has been proven well preserved (Csordas et al., 1999; Pacher et al., 2000; Csordas and Hajnoczky, 2003; Csordas et al., 2006). Also, the apparent $[Ca^{2+}]_c$ threshold for activation of the mitochondrial Ca^{2+} uptake is ~1 μM (Csordas et al., 1999; Csordas and Hajnoczky, 2001; Csordas and Hajnoczky, 2003), allowing us to selectively preload the ER using small, sub-threshold Ca^{2+} boluses. We chose 3.6 nmol $CaCl_2$ (corresponding to ~1.5 nmol/mg cellular protein in the 1.8 ml assay volume) as the maximum single-bolus, which raises $[Ca^{2+}]_{bm}$ to ≤700 nM (Figure 2A, each bolus is marked as 2Ca). For greater preload, this bolus was repeated after the first bolus was sequestered (Figure 2A Ca^{2+} preloading 3 nmol/mg). The Ca^{2+} pulses themselves caused negligible $[Ca^{2+}]_m$ increase and the decay kinetic of the associated $[Ca^{2+}]_{bm}$ elevations was well-fit by a single exponential decay, consistent with ER uptake being the dominant mechanism. $[Ca^{2+}]_c$ and $[Ca^{2+}]_m$ responses evoked by a saturating dose of IP_3 after addition of 0 to 3 pulses of $CaCl_2$ were simultaneously monitored. Increasing Ca^{2+}_{ER} by these Ca^{2+} pulses enhanced the IP_3-induced global $[Ca^{2+}]_{bm}$ response, ~2-fold increase after two Ca^{2+} pulses (Figure 2A, $[Ca^{2+}]_{bm}$, red traces), and, to a much larger extent, the associated $[Ca^{2+}]_m$ response, ~5-fold increase after two Ca^{2+} pulses (Figure 2A, $[Ca^{2+}]_m$, red traces). This pattern in the enhancement of the IP_3-induced $[Ca^{2+}]_{bm}$ and $[Ca^{2+}]_m$ responses could be consistently observed across up to three Ca^{2+} loading boluses (Figure 2B). Further Ca^{2+} addition saturated the ER capacity (not shown). Thus, in both intact and permeabilized cells increases in Ca^{2+}_{ER} increased the $[Ca^{2+}]_m$ signal more effectively than it increased the $[Ca^{2+}]_{bm}$ response during IP_3-induced Ca^{2+} release. Like in intact cells, increasing the ER Ca^{2+} preload did not enhance the mitochondrial uptake of Ca^{2+} from a non-ER source (a 10 μM $CaCl_2$ bolus, corresponding to 7.5 nmol/mg, elevated the bulk $[Ca^{2+}]_{bm}$ to ~3 μM; Figure 2A, black traces and Figure 2B) suggesting that the Ca^{2+} sensitivity of the mitochondrial Ca^{2+} uptake was unaffected.

The Steep Dependence of IP_3-Induced $[Ca^{2+}]_m$ Signals on ER Ca^{2+} Loading Relies on Local Ca^{2+} Transfer

To validate the role of the local Ca^{2+} transfer in the enhanced efficacy of IP_3-induced $[Ca^{2+}]_m$ signal generation, after different Ca^{2+} preload conditions, the $[Ca^{2+}]_{bm}$ was clamped by a slow Ca^{2+} chelator (100 μM EGTA + 30 μM $CaCl_2$ clamped $[Ca^{2+}]_{bm}$ at ≈80 nM) (Csordas et al., 1999). EGTA-clamping of $[Ca^{2+}]_c$ effectively eliminated IP_3-induced global $[Ca^{2+}]_{bm}$ increases but not the corresponding $[Ca^{2+}]_m$ responses, which were only moderately attenuated (Figure 3A, thin vs. thick traces). Moreover, the fold change in the magnitude of $[Ca^{2+}]_m$ response upon increasing the ER Ca^{2+} preload from 0 to 1.5 nmol/mg was not dampened by the $[Ca^{2+}]_{bm}$ clamping, but rather increased (470 ± 70% vs. 340 ± 30%) (Figure 3B). This result confirms that the enhancement of the $[Ca^{2+}]_m$ response occurs at the level of the activation of mitochondrial Ca^{2+} uptake sites locally by IP3R-derived high $[Ca^{2+}]$ nanodomains.

Supralinear Dependence of Mitochondrial Ca^{2+} Sequestration on the ER Ca^{2+} Pre-Loading During IP_3-Induced Ca^{2+} Release

The steep enhancement of the IP3R-linked $[Ca^{2+}]_m$ signals with increasing Ca^{2+} loading of the ER raised the possibility of increasingly efficient mitochondrial Ca^{2+} clearance around the ER Ca^{2+} release sites. To directly address this point, we set up a strategy to quantify the amount of mitochondrial Ca^{2+} uptake associated with IP_3-induced Ca^{2+} release at different Ca^{2+}_{ER} loads (established via preloading with 0, 0.375, 0.75, 1.5, and 3 nmol/mg Ca^{2+}) in suspensions of permeabilized cells. The quantification procedure is illustrated in Figure 4A. In the permeabilized RBL-2H3 cells, ER and mitochondria dominate the Ca^{2+} handling (Csordas and Hajnoczky, 2001). When Ca^{2+} accumulation to these organelles is blocked (SERCA by thapsigargin, Tg, added just 5 s before IP_3 addition, and mitochondrial uptake by uncoupler FCCP/oligomycin or ruthenium red), the initial rise in $[Ca^{2+}]_{bm}$ in response to IP_3 is solely derived from the release flux via the IP3R (red traces and double-headed arrows in Figure 4A, bottom panels). Supramaximal IP_3-addition elicited complete discharge of the ER Ca^{2+} store as evidenced by the lack of further $[Ca^{2+}]_{bm}$ increase upon addition of the Ca^{2+} ionophore ionomycin (Figure 4A, right). When mitochondrial Ca^{2+} uptake is not blocked, the IP_3-induced $[Ca^{2+}]_{bm}$ rise will be smaller, since a portion of the released Ca^{2+} from the ER is sequestered by the mitochondria (black traces and opposing inward arrows in Figure 4A, bottom panels). In turn, based on titration of the $[Ca^{2+}]_{bm}$ changes with known amounts of Ca^{2+} (Figure 4B), the molar Ca^{2+} content of the ER (Ca^{2+}_{ER}) as well as the Ca^{2+} sequestered by the mitochondria during IP_3-induced Ca^{2+} release was determined. Importantly, the IP_3-induced Ca^{2+} release was completed by the end of the rapid upstroke phase of the $[Ca^{2+}]_{bm}$ increase (in ~2.5–5 s, calculated from the first derivative), regardless of the ER Ca^{2+} load (Figure 4A, inset). Accordingly, IP3R-derived high $[Ca^{2+}]$ nanodomains could only exist during this period, and so we limited the evaluation of mitochondrial Ca^{2+} uptake to this initial interval (ignoring further slow uptake from the global $[Ca^{2+}]_{bm}$ rise likely due to a long-term uniporter sensitization; Csordas and Hajnoczky, 2003). As expected, Ca^{2+}_{ER} increased linearly with the Ca^{2+} loading amounts (with a slope ~1), further reflecting that the added Ca^{2+} was deposited entirely to the rapidly mobilizable ER Ca^{2+} pool (Figure 5A,

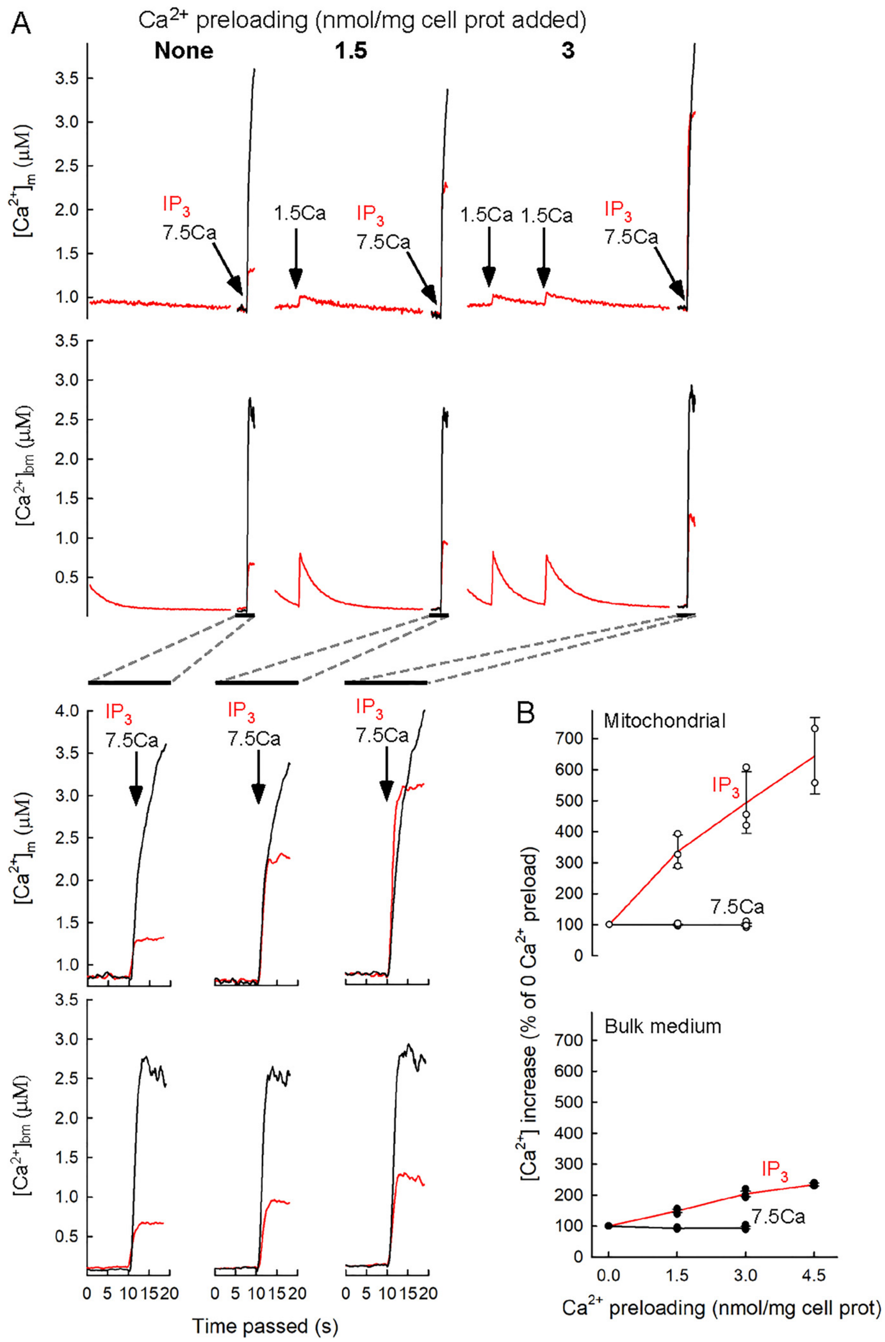

Figure 2. Enhancement of the IP_3-Induced $[Ca^{2+}]_c$ and $[Ca^{2+}]_m$ Responses by Increasing ER Ca^{2+} Load in Permeabilized Cells.
In suspensions of permeabilized cells, $[Ca^{2+}]_{bm}$ and $[Ca^{2+}]_m$ were monitored fluorometrically using rhod-2 (free acid) dissolved in the cytosolic buffer and fura-2FF compartmentalized in the mitochondria, respectively. Ca^{2+} loading of the ER was allowed to happen from the cytosolic buffer either without additional Ca^{2+} or by applying 2 μM $CaCl_2$ ($2Ca^{2+}$) boluse(s). IP_3 (10 μM) stimulation was applied 150–180 s after the last $CaCl_2$ pulse. In parallel experiments 10 μM $CaCl_2$ ($10Ca^{2+}$) bolus was used to stimulate mitochondrial Ca^{2+} uptake instead of IP_3. (A) Representative analog recordings of $[Ca^{2+}]_{bm}$ and $[Ca^{2+}]_m$ during the Ca^{2+} loading period (before break) and the responses to IP_3 (post-break red traces) or to 10Ca (post-break black traces). Since preloading was identical for IP_3 and 10Ca, for better clarity, the representative trace is only shown for one (IP_3). Recordings are shown without Ca^{2+} preloading (none), after one and two $2Ca^{2+}$ pulses (Ca^{2+} preloading 1.5 and 3 nmol/mg cellular protein, respectively). Post-break periods on expanded time scale are shown underneath as indicated. The post-stimulation time window is 10 s, in which the IP3R-mediated Ca^{2+} release and corresponding rapid phase of mitochondrial Ca^{2+} uptake are completed ($[Ca^{2+}]_{bm}$ responses to both, IP_3 and $10Ca^{2+}$, are in the post-peak decline/plateau phase and red traces of $[Ca^{2+}]_m$ responses to IP_3 are past the relatively large rapid upstrokes, and show only minor updrifts). (B) Cumulated $[Ca^{2+}]_{bm}$ and $[Ca^{2+}]_m$ increases evoked by IP_3 or 10 μM $CaCl_2$ under different ER Ca^{2+}-preloading conditions. Data are normalized to the condition when no $CaCl_2$ pulse was applied prior to stimulation (means + S.E., $N = 3$ independent experiments).

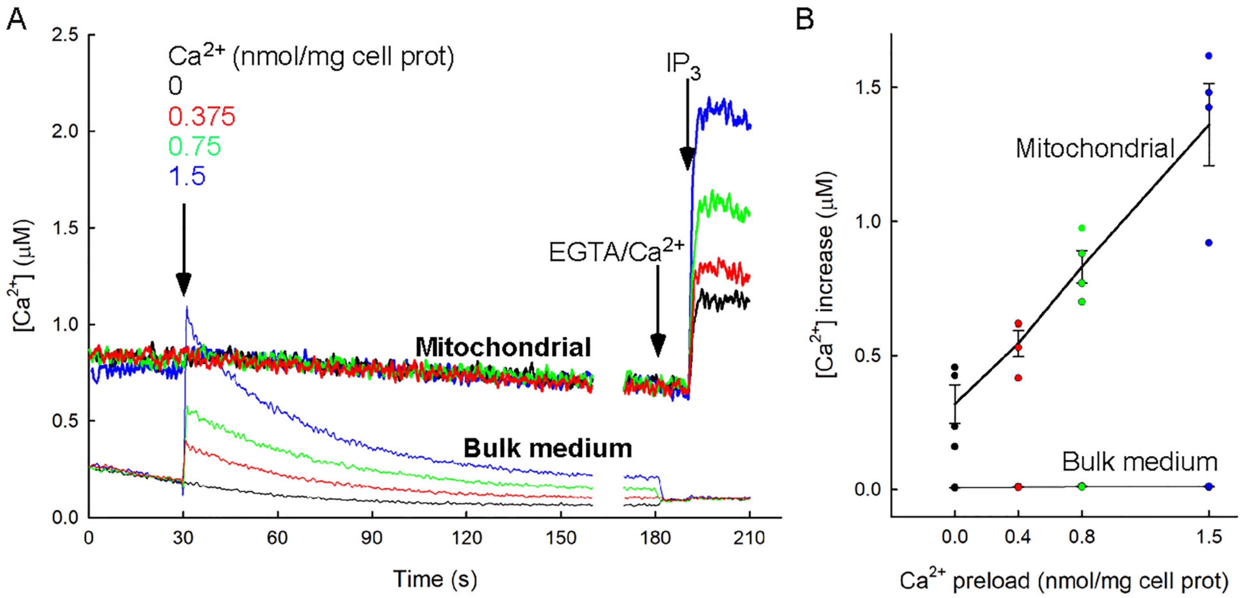

Figure 3. Increased Ca^{2+} Loading of the ER Enhances the IP_3-Induced $[Ca^{2+}]_m$ Response Even if $[Ca^{2+}]_{bm}$ is Clamped With EGTA in Suspensions of Permeabilized RBL-2H3 Cells.
In suspensions of permeabilized RBL-2H3 cells, ER Ca^{2+} loading was controlled by single boluses of added $CaCl_2$ (Ca^{2+} 0, 0.375, 0.75, 1.5 nmol/mg as labeled), while $[Ca^{2+}]_{bm}$ and $[Ca^{2+}]_m$ were fluorometrically recorded. 30 s before IP_3 (10 µM) stimulation, $[Ca^{2+}]_c$ was clamped to ∼80–100 nM by the addition of a mixture of EGTA/$CaCl_2$ (100 µM/30 µM, respectively). (A) Time courses of $[Ca^{2+}]_{bm}$ (hairline) and $[Ca^{2+}]_m$ (mitochondrial, thick lines) color coded for the different Ca^{2+} preloading pulses used (as indicated). (B) $[Ca^{2+}]_m$ increases evoked by IP_3 plotted against the different ER Ca^{2+}-preloading conditions from the experiments shown in (A) (means + S.E., $N = 3$ independent experiments).

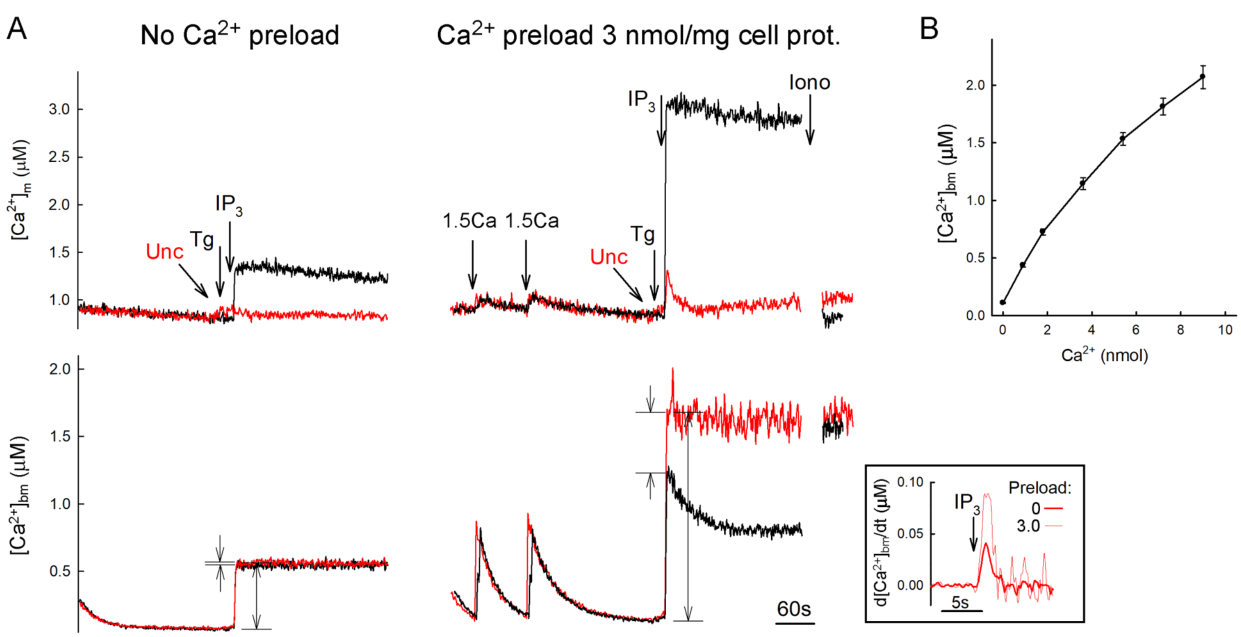

Figure 4. Quantification of ER Ca^{2+} Content and Mitochondrial Ca^{2+} Uptake Associated With IP_3-Induced Ca^{2+} Release.
(A) IP_3-induced $[Ca^{2+}]_{bm}$ and $[Ca^{2+}]_m$ increases in suspensions of permeabilized cells were recorded as in Figure 1 in the presence (red traces) and absence (black traces) of mitochondrial uncoupler (Unc: FCCP/oligomycin 2 µM/5 µg/mL). Tg (2 µM) was applied 5 s before IP_3 (10 µM) stimulation to prevent Ca^{2+} reuptake to the ER. $[Ca^{2+}]_{bm}$ increase evoked by IP_3 in the presence of uncoupler (depicted by outward double arrows) reflects the Ca^{2+} amounts stored in the ER. The difference between IP_3-induced $[Ca^{2+}]_{bm}$ increases in the presence and absence of uncoupler (depicted by inward double arrows) reflects the Ca^{2+} amounts taken up by the mitochondria. Inset: first derivatives of the IP_3-induced $[Ca^{2+}]_{bm}$ responses in the presence of uncoupler. (B) Titration curve of $[Ca^{2+}]_c$ elevations with known amounts of Ca^{2+}.

Dataset S1). Mitochondrial Ca^{2+} uptake from the IP_3-induced Ca^{2+} release showed massive enhancement with the increases in ER Ca^{2+} preloading (Figure 4A, bottom). Consistently, the amounts of Ca^{2+} sequestered by mitochondria during IP_3-induced Ca^{2+} release displayed a supralinear correlation with Ca^{2+}_{ER} that was best fitted with a single-exponential growth curve in the tested range of ER Ca^{2+} content (Figure 5B, Dataset S1). Accordingly, the fractional of the released Ca^{2+} sequestered by mitochondria increased with Ca^{2+}_{ER} (Figure 5C, Dataset S1). Thus, increasing the Ca^{2+}_{ER} improved the efficacy of IP3R-dependent local Ca^{2+} delivery to the mitochondria.

Sigmoidal Dependence of the IP_3-Induced $[Ca^{2+}]_m$ Response on ER Ca^{2+} Loading

While mitochondrial Ca^{2+} uptake during the IP_3-stimulated Ca^{2+} release progressively increased across the tested range of Ca^{2+}_{ER}, the corresponding $[Ca^{2+}]_m$ increases displayed more complex kinetics. Up until Ca^{2+}_{ER} of ~1.7 nmol/mg cellular protein, $[Ca^{2+}]_m$ responses were increasing progressively, but then they turned to saturation with a kinetics best fitted with a three-parameter sigmoidal curve (Figure 6A, Dataset S1). Accordingly, plotting IP_3-induced Ca^{2+} release-associated $[Ca^{2+}]_m$ increases against the corresponding mitochondrial Ca^{2+} uptake displayed simple saturation kinetics (Figure 6B, Dataset 1), suggesting the presence/activation of a low-affinity, high-capacity $[Ca^{2+}]$ buffer species in the mitochondrial matrix (David, 1999; Nicholls, 2005). Since the saturating $[Ca^{2+}]_m$ values over the sigmoidal curve were just around the K_d value of the Ca^{2+} probe fura-2FF/fura-loAff (4.5 μM), saturation of the dye or contribution by the dye to the maximal $[Ca^{2+}]$ as a chelator was unlikely. Thus, amplitude modulation of the $[Ca^{2+}]_m$ signals by mitochondrial Ca^{2+} uptake takes place only in a limited range, beyond which the sequestered Ca^{2+} is mostly chelated by powerful Ca^{2+} buffering in the matrix.

IP3R-Derived High $[Ca^{2+}]$ Nanodomains at the Mitochondrial Surface Linearly Depend on Ca^{2+}_{ER}

To obtain clues about where the Ca^{2+}_{ER}-dependent amplification takes place along the route of Ca^{2+} from the IP3Rs to the mitochondrial matrix, we first examined how the IP3R-derived high $[Ca^{2+}]_c$ nanodomains exposing the mitochondrial surface are determined by Ca^{2+}_{ER}. To measure local $[Ca^{2+}]$ at the ER-mitochondria contacts, we used a drug-inducible bipartite inter-organellar linker system based on the heterodimerization of FKBP12 and FRB protein domains via rapamycin (Csordas et al., 2010). A low-affinity fluorescent Ca^{2+} indicator protein RCaMP ($RCaMP^{R368V}$, RCaMPv) was used as a tag on FKBP12 anchored to the outer mitochondrial membrane (OMM) via the membrane insertion domain of mAKAP1 (mAKAP1(34-64)) (OMM-FKBP-RCaMPv). The linkage partner FRB domain was anchored to the ER via the membrane insertion domain of Sac1 and a 9x flexible helical repeat and tagged with a cyan fluorescent protein (CFP-FRB-9x-Sac1). Rapamycin treatment (5 min) immobilized OMM-FKBP-RCaMPv at the close contacts with the ER by linkage with the CFP-FRB-9x-Sac1 in the ER (Csordas et al., 2010; Csordas et al., 2013).

To vary Ca^{2+}_{ER}, $[Ca^{2+}]_c$ was stepped up from a nominally Ca^{2+}-free baseline (10 μM EGTA in the buffer) to ~200 nM (addition of 3 μM $CaCl_2$) for various durations before discharging the ER store by saturating $[IP_3]$. Figure 7A shows the kinetics of $[Ca^{2+}]$ rises detected by the OMM-FKBP-RCaMPv recruited to the close contacts with ER ($[Ca^{2+}]_{OMM-ER}$). The IP_3-induced $[Ca^{2+}]_{OMM-ER}$ spikes were asymmetrical, comprised of a rapid upstroke to the peak followed by a rapid drop that slowed when approaching the baseline, reaching ≥80% recovery in 30 s. Similarly to cells in suspension, where the store depletion upon IP3R stimulation was completed in <5 s regardless of store loading (Figure 4A, inset), the time-to-peak remained <5 s regardless of the duration of the ER Ca^{2+} loading period (Figure 7B). For estimating the time-dependent increases in Ca^{2+}_{ER} the area under curve of the $[Ca^{2+}]_{OMM-ER}$ response was used (Figure 7C). The increases in the area under curve involved increases in peak amplitudes and slower recovery. They fitted well with a saturation curve, consistently with the time-dependent (re)filling of the finite ER Ca^{2+} pool (Figure 7C, Dataset S1). To stay consistent with the cell suspension assays, where only the initial steep phase of the mitochondrial Ca^{2+} uptake was counted, we considered the $[Ca^{2+}]_{OMM-ER}$ peak amplitudes as the relevant parameters of the nanodomains to describe the contribution to the initial activation of the mitochondrial Ca^{2+} uptake. By contrast to the supralinearly increasing mitochondrial uptake, the increase of $[Ca^{2+}]_{OMM-ER}$ peaks with the growing Ca^{2+}_{ER} (area under curve) could be approximated by a linear fit (Figure 7D, right, Dataset S1). Admittedly, reflecting the ER Ca^{2+} load by the area of the local calcium rise shown by RCaMP has limitations that are further considered in the methods. Regardless, the $[Ca^{2+}]_{OMM-ER}$ does not seem to be a non-linear amplifying factor in the process of progressive activation of mitochondrial Ca^{2+} uptake by IP3R-mediated Ca^{2+} release at increasing Ca^{2+}_{ER}.

MICU1 in the mtCU Likely Acts as a $[Ca^{2+}]$-Dependent Amplifier

After finding no evidence for a "pre-mitochondrial" Ca^{2+}_{ER}-dependent supralinear amplifier in the local IP3R-to-mitochondria Ca^{2+} transfer, we examined the mitochondrial Ca^{2+} uptake machinery. We focused on MICU1, the Ca^{2+}-sensing regulatory subunit of mtCU in the mitochondrial intermembrane space, which is essential for the cooperative activation of the mtCU by Ca^{2+} binding to its EF hand domains (Csordas et al., 2013; Logan et al., 2014; Patron et al., 2014). Because stable knockdown of MICU1 was not

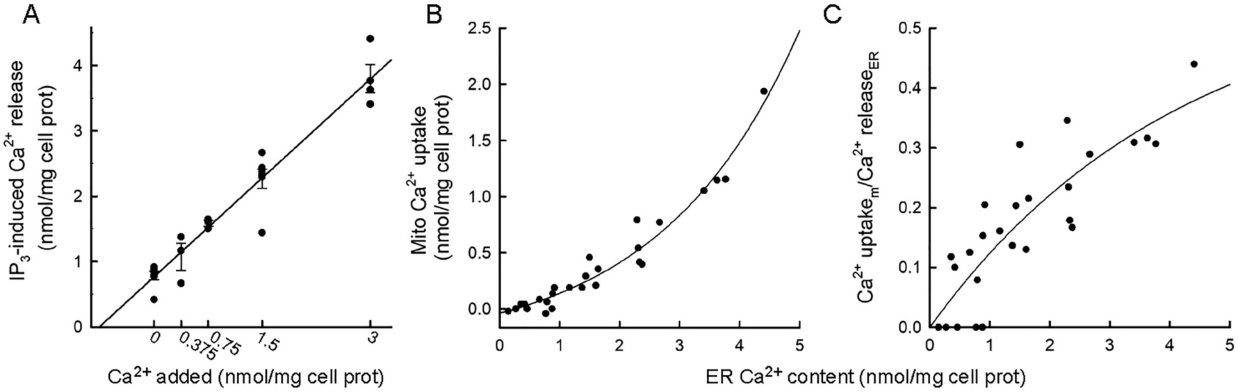

Figure 5. Supralinear Relationship Between the ER Ca^{2+} Content and the Mitochondrial Ca^{2+} Uptake Associated With IP_3-Induced Ca^{2+} Release.
ER Ca^{2+} content and the associated mitochondrial Ca^{2+} uptake were calculated from pairs of recordings (w/wo uncoupler). (A) ER Ca^{2+} content as a function of the Ca^{2+} amounts added to the system (in the form of $CaCl_2$ pulses). The slope of the linear fit (m) is ~1. (B,C) Total (middle) and fractional (right) mitochondrial Ca^{2+} uptake from IP_3-induced Ca^{2+} release as a function of ER Ca^{2+} content ($n = 7$).

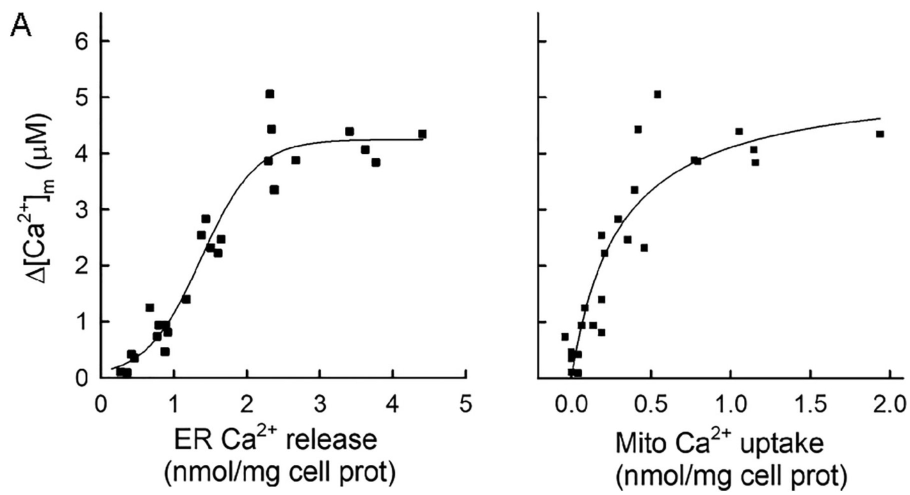

Figure 6. Dependence of the IP_3-Induced $[Ca^{2+}]_m$ Rise on ER Ca^{2+} Content.
(A) The magnitudes of $[Ca^{2+}]_m$ responses associated with IP_3-induced Ca^{2+} release plotted against the corresponding ER Ca^{2+} contents. (B) $[Ca^{2+}]_m$ response associated with IP_3-induced Ca^{2+} release plotted against the corresponding mitochondrial Ca^{2+} uptake. Data are from the same experiments as in Figure 5.

successful in RBL-2H3 cells, we compared the correlation between the $[Ca^{2+}]_c$ and $[Ca^{2+}]_m$ increases associated with SOCE between control cells and cells transiently overexpressing a mutant MICU1 with both Ca^{2+}-binding EF hands incapacitated (MICU1ΔEF1,2; Perocchi et al., 2010). We predicted MICU1ΔEF1,2 to work as dominant negative with regard to the cooperative activation of mtCU (Csordas et al., 2013) (for potential mechanisms, see Discussion). Time courses showed a substantial lag between the start of $[Ca^{2+}]_c$ and $[Ca^{2+}]_m$ rises in the control cells. $[Ca^{2+}]_m$ started to rise abruptly by the time $[Ca^{2+}]_c$ was already over half-way to its peak and it reached plateau about as fast as $[Ca^{2+}]_c$ (hence the rapid rising phases are parallel in Figure 8A left, where the *y*-axes are scaled to fully expand the basal-to-peak range). By contrast, in the MICU1ΔEF1,2 overexpressing cells the $[Ca^{2+}]_m$ rise started together with the $[Ca^{2+}]_c$ rise; however, the rate of $[Ca^{2+}]_m$ rise to the peak was slower than that for $[Ca^{2+}]_c$. Accordingly, the $[Ca^{2+}]_m$ versus $[Ca^{2+}]_c$ plots started to rise at higher $[Ca^{2+}]_c$ in the control cells, but with a relatively sharp transition to the rising phase (Figure 8B). The $[Ca^{2+}]_m$ versus $[Ca^{2+}]_c$ plots could be fit by single exponentials for both control and MICU1ΔEF1,2 overexpressing cells but the rate constants of the curve fitting equations in the MICU1ΔEF1,2 cells were nearly half of that in the control cells (Figure 8C). Thus, the mtCU showed diminished cooperativity in the Ca^{2+}-activation in the MICU1ΔEF1,2 overexpressing cells. These results suggest that MICU1 serves as a non-linear amplifier of the $[Ca^{2+}]_c$ signals propagated to the

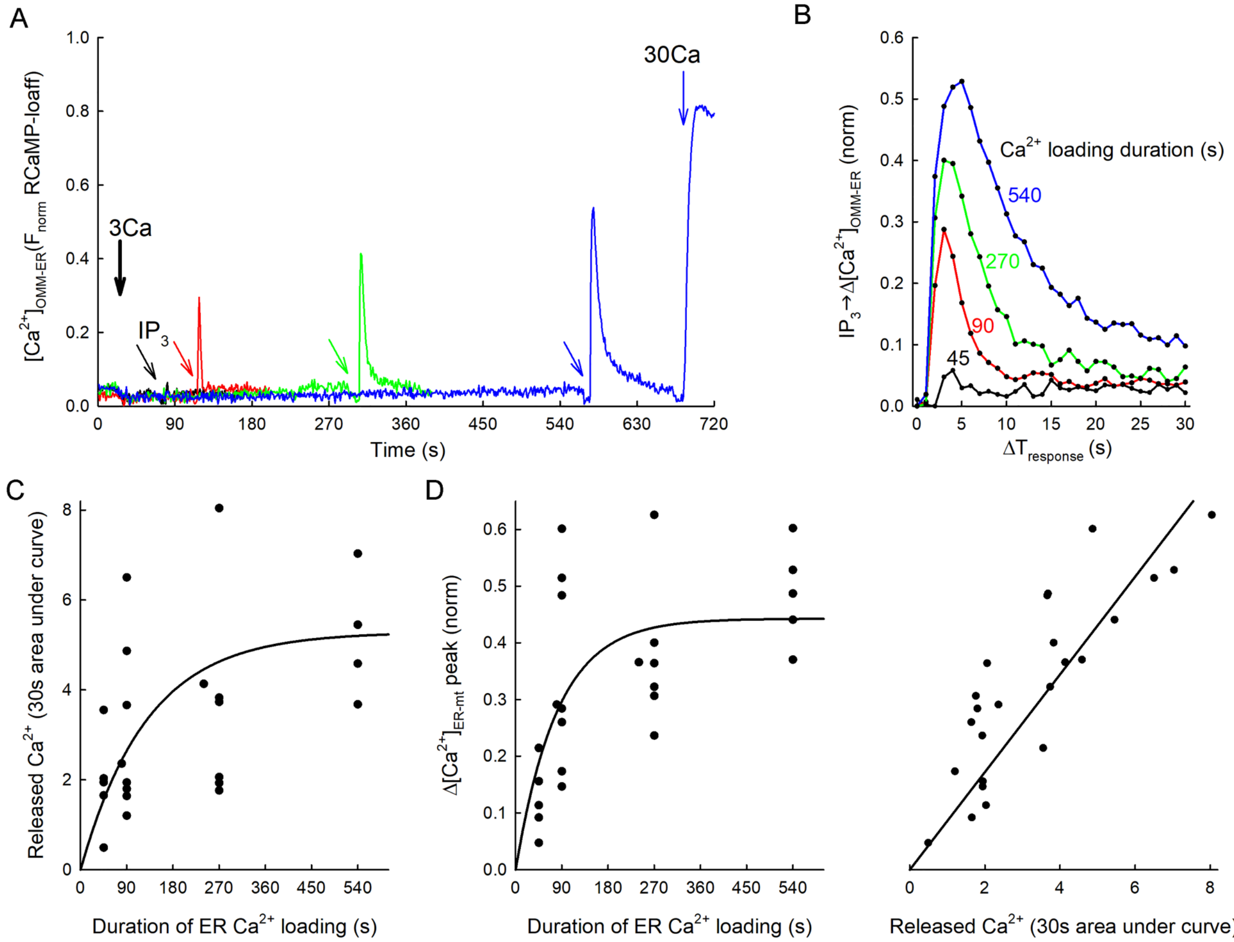

Figure 7. Correlation of IP3R-Derived High $[Ca^{2+}]$OMM-ER Microdomain Peaks With Ca^{2+}_{ER}.
High $[Ca^{2+}]_{OMM-ER}$ microdomains exposing the mitochondrial surface at close interfaces with the ER upon maximum IP3R stimulation (IP_3 10 μM + Tg 2 μM, IP_3) were measured using OMM-targeted RCaMPloaff recruited to site via rapamycin-inducible intermembrane cross-bridging (see Methods) in permeabilized RBL-2H3 cells. Grading of Ca^{2+}_{ER} was achieved by varying the duration (45 s, 90 s, 270 s, 540 s) of loading via elevating bath $[Ca^{2+}]$ from nominally 0 (EGTA 10 μM, no added Ca^{2+}) to ~200 nM (adding $CaCl_2$ 3 μM, 3Ca). (A) Representative time courses (mean traces of 10–20 individual cells) of the recorded $[Ca^{2+}]_{OMM-ER}$ changes. RCaMPv fluorescence is normalized to the total Ca^{2+} sensitive range (see Methods). Color-matched tilted arrows show the time of IP3 addition. (B) IP3-induced $[Ca^{2+}]_{OMM-ER}$ responses after the different lengths of ER Ca^{2+} loading (as indicated by the numbers) synchronized to the time of IP3 addition. Note that peaks are reached essentially at the same time in all. (C) Area under curve values for the IP3-induced $[Ca^{2+}]_{OMM-ER}$ responses (initial 30 s, used as an approximation for Ca^{2+}_{ER}) plotted against the duration of Ca^{2+} loading and fitted (best) with a single-exponential rise to maximum curve $f = a(1\text{-}e^{-bx})$. Like the traces in AB, each point represents the mean of 10–20 individual cells from a single recording. (D) Peak magnitudes of IP_3-induced $[Ca^{2+}]_{OMM-ER}$ microdomain responses plotted against the duration of Ca^{2+} loading (left, fitted with single-exponential rise to maximum curve) and against the released Ca^{2+}_{ER} as assessed by the area under curve (right, fitted best with linear).

mitochondrial matrix, and as such, MICU1 likely contributes to the store content-dependent enhancement of the efficacy of local Ca^{2+} transfer from the IP3R to the mitochondria.

Discussion

We aimed to establish the relationship between ER Ca^{2+} loading state (Ca^{2+}_{ER}) and the efficacy of local Ca^{2+} delivery from IP3Rs to the mitochondrial matrix. Quantification of the ER luminal $[Ca^{2+}]$ ($[Ca^{2+}]_{ER}$) has been reported before but it does not provide direct assessment of the amount of Ca^{2+} transferred to the cytoplasm and the mitochondrial matrix, because of the different Ca^{2+} binding species in each compartment. We think our measurements have achieved the goal of quantitatively measuring the amounts of Ca^{2+} locally transported to the mitochondria at the ER-mitochondrial contacts during IP3R activation, which is central to understanding the mechanism of Ca^{2+} transfer and has never been realized.

Positive dependence of IP3R-dependent $[Ca^{2+}]_m$ signals on ER Ca^{2+} levels has been speculated based on

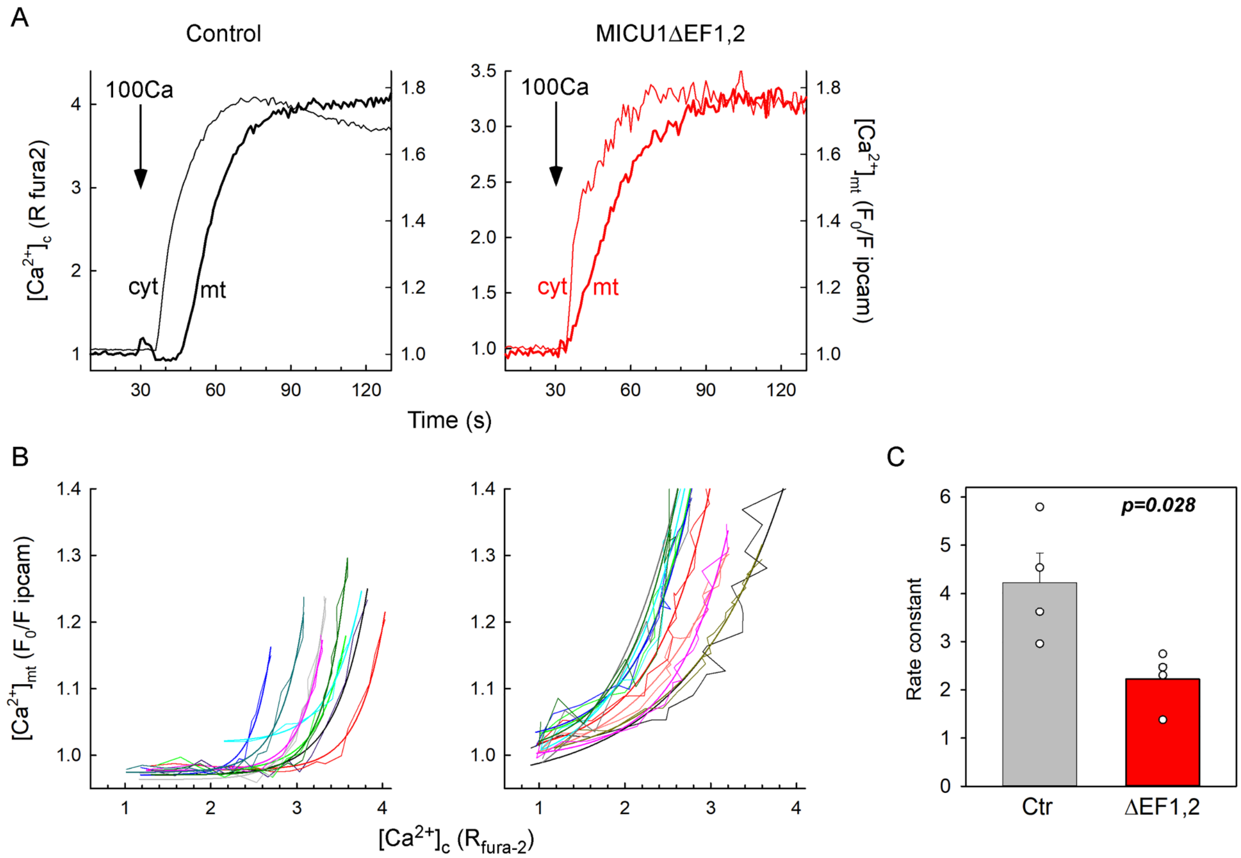

Figure 8. Cooperative Activation of Mitochondrial Ca^{2+} Signals During SOCE is Compromised in EF-Mutant MICU1 Overexpressing Cells.
RBL-2H3 cells were transiently transfected with mitochondrial matrix-targeted inverse pericam along with the double-EF-hand mutant MICU1 (MICU1ΔEF1,2) or without it (control). SOCE-associated $[Ca^{2+}]_c$ and $[Ca^{2+}]_m$ signals were simultaneously recorded via fluorescence microscopic imaging of fura-2 and ipcam signals, respectively. SOCE channels were activated by Ca^{2+} depletion of the ER (Tg 2 μM pretreatment) in the absence of extracellular Ca^{2+}. Ca^{2+} entry was started by the addition of a 100 mM $CaCl_2$ bolus (100Ca). (A) Representative time courses (mean traces of 10–18 individual cells). $[Ca^{2+}]_m$ responses (thick lines) are scaled equally between control (left) and MICU1ΔEF1,2 (right); whereas $[Ca^{2+}]_c$ responses (thin lines) are scaled to have their baseline and maximum values aligned with $[Ca^{2+}]_m$. Note the delayed onset of $[Ca^{2+}]_m$ response in the control but not in the MICU1ΔEF1,2 cells on one hand, but also the slower rising kinetics in MICU1ΔEF1,2 on the other hand. (B) $[Ca^{2+}]_m$ versus $[Ca^{2+}]_c$ plots from the cells in (A), truncated to expose the transition from post Ca^{2+}-addition to the rising phase and fitted with single-exponential growth curves ($f = y_0 + ae^{bx}$). The rate constants (b) cumulated from four separate recordings are shown in (C). * denotes significant difference in the means as determined by *t*-test ($p = .026$).

circumstantial evidence (Ma et al., 1999; Foyouzi-Youssefi et al., 2000; Pinton et al., 2000, 2001; Spat et al., 2008) (Some of the present results were cited as unpublished in a review, Spat et al., 2008). Here we report in intact RBL-2H3 cells that the $[Ca^{2+}]_m$ signals evoked by the IP3R-mediated Ca^{2+} release are more sensitive than the $[Ca^{2+}]_c$ signals to ER Ca^{2+} loading, at least in its physiological range. These results extend earlier findings that interference with submaximal IP3R activation via overexpression of IP_3 buffers (Lin et al., 2005) or with TGFβ treatment (Pacher et al., 2008) affected $[Ca^{2+}]_m$ signals more profoundly than the $[Ca^{2+}]_c$ signals. To directly assess the correlation between Ca^{2+}_{ER} and the IP3R-to-mitochondria Ca^{2+} transfer, we used permeabilized cells, in which Ca^{2+}_{ER} content could be quantitatively controlled and both the mitochondrial uptake as well as $[Ca^{2+}]_m$ signals during IP3R activation could be quantified. The observed relationships among ER Ca^{2+} load, IP_3-induced Ca^{2+} release, global and local $[Ca^{2+}]_c$ rise, mitochondrial Ca^{2+} uptake, and $[Ca^{2+}]_m$ rise are summarized in Figure 9. This analysis and the mechanistic clues provided by our study are expected to help the interpretation of the findings of a broad range of studies focusing on ER stress and other conditions altering ER Ca^{2+} storage.

Loading with repetitive small Ca^{2+} pulses increased the Ca^{2+}_{ER} storage linearly to at least 3.8 nmol Ca^{2+} per mg cellular protein (Figure 9i). The ER Ca^{2+} content was approximated by the Ca^{2+} discharged by maximal IP_3, under SERCA inhibition, and it appeared in a linear relationship with both, the global and local $[Ca^{2+}]_c$ increases

(Figure 9ii), whereas the increases in Ca^{2+}_{ER} supralinearly enhanced the mitochondrial Ca^{2+} uptake (Figure 9iii). As to the IP3R-mediated $[Ca^{2+}]_m$ signal, up until 1.5 nmol Ca^{2+}_{ER}/mg protein the rise was supralinear, whereas further increases in Ca^{2+}_{ER} were meeting an apparent plateau of the IP_3-induced $[Ca^{2+}]_m$ signal (at ∼3–4 μM) (Figure 9iv). The sublinear (saturation) correlation between IP_3-induced mitochondrial Ca^{2+} uptake and the corresponding $[Ca^{2+}]_m$ signal at higher Ca^{2+}_{ER} (Figure 9v) was likely due to Ca^{2+} buffering in the mitochondrial matrix. This buffering system does not seem to allow $[Ca^{2+}]_m$ to rise much beyond the reported activation range of matrix Ca^{2+} sensitive dehydrogenases ($K_{[Ca2+]}$ ∼ 1 μM, Denton and McCormack, 1986) perhaps to keep $[Ca^{2+}]_m$ below the "danger zone" for mPTP induction (Bernardi, 2013). The IP3R-mitochondrial local Ca^{2+} transfer thus provided (i) Ca^{2+}_{ER}-dependent amplitude modulation of IP3R-linked $[Ca^{2+}]_m$ signals in the relevant range to regulate matrix dehydrogenases but also (ii) optimal support for the mitochondria to maintain their "Ca^{2+} sink" function. Similar plateau/saturation in the $[Ca^{2+}]_m$ due to matrix Ca^{2+} buffering during continuing mitochondrial Ca^{2+} clearance have been reported in association with Ca^{2+} entry in motor neurons (David, 1999) or in suspensions of liver, brain (Nicholls and Chalmers, 2004), and heart (Bazil et al., 2013; Wei et al., 2012) mitochondrial fractions. Identification of the buffer species responsible for the complex behavior of $[Ca^{2+}]_m$ is yet to be elucidated but P_i likely contributes to the buffering as P_i deprivation alleviates the $[Ca^{2+}]_m$ limit in most of the paradigms tested

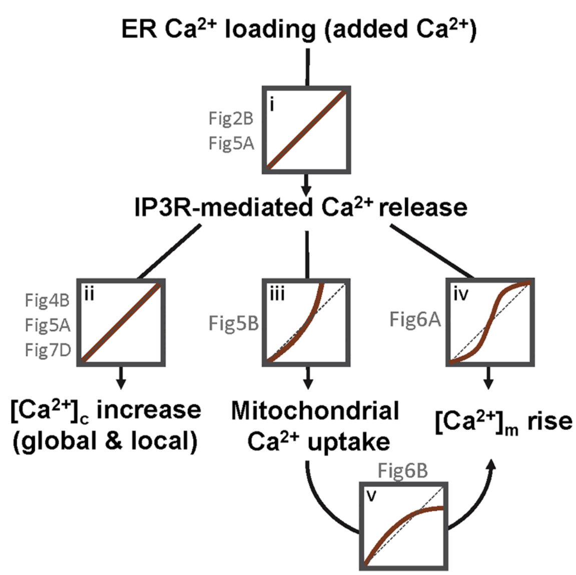

Figure 9. Schematic Presentation of the ER Ca^{2+} Dependence of Each Step in Calcium Signal Propagation From the IP3R to the Mitochondria.
Arrows show the quantitatively assessed relationships among the steps in the pathway and schematized kinetics traces indicate the findings on these relationships, whereas the source figure for each is cited by gray characters.

(Chalmers and Nicholls, 2003; de la Fuente et al., 2012; Wei et al., 2012; Bazil et al., 2013) Although most Ca^{2+} indicator dyes are based on Ca^{2+} chelators (BAPTA), Fura2FF loaded to the mitochondrial matrix (fura-2FF) is not likely a significant contributor to the observed matrix Ca^{2+} buffering that caused a plateau in the $[Ca^{2+}]_m$ versus Ca^{2+}_m curves given that the plateau occurred at $[Ca^{2+}]_m$ levels around the K_d value (∼4.5 μM), where the fluorescence is the most sensitive to report changes in the Ca^{2+}-bound form of the dye. The maximal $[Ca^{2+}]_m$ is determined by the endogenous buffers. Notably, the $[Ca^{2+}]_m$ "working range" determined in our study matches well $[Ca^{2+}]_m$ that have been measured previously by fluorescent Ca^{2+} probes (David et al., 2003) and Ca^{2+} sensing fluorescent proteins (Suzuki et al., 2014) but is lower than what was reported using aequorin as Ca^{2+} sensor (Montero et al., 2000; Tosatto et al., 2017). The reason for these discrepancies remains elusive.

The IP3R-mediated complete discharge of the ER store did not require more time at increased ER Ca^{2+} load, presumably because of the positive effect of ER luminal Ca^{2+} on the Ca^{2+} flux by the IP_3-bound IP3R (Missiaen et al., 1992; Oldershaw and Taylor, 1993; Horne and Meyer, 1995). This feature may be needed for effective amplitude modulation of the IP3R-derived high $[Ca^{2+}]_c$ microdomains since activated IP3Rs undergo time-dependent inactivation (Hajnoczky and Thomas, 1994), that is, the release of larger Ca^{2+} loads should not last longer since the longer release time would mean progressively decreasing IP3R channel activities.

We wanted to identify the specific Ca^{2+}_{ER}-dependent supralinear amplification point in the IP3R-to-mitochondria local Ca^{2+} transfer. From the ER lumen to the mitochondrial matrix, Ca^{2+} has to cross three membranes: the ER (via the IP3R), the OMM (mostly through VDACs), and the IMM (via the uniporter, mtCU). The local Ca^{2+} transfer also depends on close contacts between subdomains of ER and mitochondria secured by protein tethers (Csordas et al., 2006; Szabadkai et al., 2006; de Brito and Scorrano, 2008). At these contact areas, the peri-mitochondrial $[Ca^{2+}]$ can reach >10 fold higher values than the bulk cytoplasm upon stimulation with IP_3-mobilizing agonists (Csordas et al., 2010; Giacomello et al., 2010). Since the time of complete store discharge remained the same throughout the tested range of Ca^{2+}_{ER} in permeabilized cells, the Ca^{2+} flux underlying the IP3R-derived high $[Ca^{2+}]$ microdomains must have followed Ca^{2+}_{ER} linearly. In theory, differences in the distribution pattern of the IP3Rs could result in $[Ca^{2+}]$ microdomains that would be more or less directed to the mitochondria. Type 3 IP3Rs have been proposed to preferentially locate to the ER-mitochondrial interface (Mendes et al., 2005) where they can be protected from proteasomal degradation by a novel chaperone complex (Sigma-1 receptor and BiP) in a $[Ca^{2+}]_{ER}$ dependent manner (Hayashi and Su, 2007). However, this mechanism protected IP3Rs more at lower $[Ca^{2+}]_{ER}$ levels and not vice versa. Ca^{2+}-dependent clustering of the IP3R has also been proposed but this process depended on $[Ca^{2+}]_c$ changes and became apparent several minutes after agonist stimulation (Wilson et al., 1998). More recently, in a systematic comparison of every IP3R isoform, we found that each isoform can support ER-mitochondrial contacts and Ca^{2+} transfer but IP3R2 has some advantages over the other isoforms (Bartok et al., 2019; Katona et al., 2022). Here, in cells that mostly express IP3R2, we have carried out direct monitoring of the IP3R-derived high $[Ca^{2+}]_{OMM\text{-}ER}$ microdomains at different ER loadings and found the peak amplitudes of the nanodomains to linearly depend on Ca^{2+}_{ER} (Figure 7). Thus, a supralinear amplification point is absent in the pre-mitochondrial steps of calcium signal propagation to the mitochondria.

Another potential amplifying factor could have been the expansion or tightening of the close ER-mitochondrial interfaces upon increased Ca^{2+}_{ER}. Disruption of ER-mitochondrial tethers enzymatically in RBL-2H3 cells (Csordas et al., 2006) or genetically in MEFs and HEK cells (Mfn2 KO, de Brito and Scorrano, 2008) diminished the IP3R-mitochondria local Ca^{2+} transfer (for recent reviews, see Csordas et al., 2018; Scorrano et al., 2019). Tightening and expanding the ER-mitochondrial contacts via synthetic tethers did not enhance the local delivery of maximal IP_3-induced Ca^{2+} signals to the mitochondria in RBL-2H3 cells suggesting that they were already positioned optimally (Csordas et al., 2006). Significant expansion of ER-mitochondrial close interfaces via rapamycin-inducible genetically engineered linkers usually requires >5 min of treatment in intact cells (Csordas et al., 2010; Booth et al., 2016). Also, motility of ER and mitochondria, a prerequisite for the expansion of close ER-mitochondrial associations, is reduced upon $[Ca^{2+}]_c$ increase and upon cell permeabilization (Yi et al., 2004), which was completed at the end of the rapamycin treatment. Thus, it is unlikely that significant expansion of the ER-mitochondrial interface occurred in the permeabilized cells during the addition of the small $CaCl_2$ boluses to load the ER. Moreover, decreased ER Ca^{2+} load associated with tunicamycin-induced ER stress resulted in expanded and tighter ER-mitochondrial associations (Csordas et al., 2006), which would indicate an inverse correlation between Ca^{2+}_{ER} and ER-mitochondrial interface formation. In sum, ER-mitochondrial interface formation is unlikely to serve as an amplifier in the correlation between Ca^{2+}_{ER} and the IP3R-mitochondrial local Ca^{2+} delivery.

The next potential amplification site is at the OMM, where VDAC channels mediate the Ca^{2+} transfer. Since the OMM has a high VDAC density, and each VDAC represents large Ca^{2+} conductance, for a long time the OMM was considered freely permeable to Ca^{2+}. More recent evidence suggests that the availability of VDAC may in fact limit local Ca^{2+} delivery (Csordas et al., 2002; Rapizzi et al., 2002) and VDAC reconstituted to liposomes has been reported to display a Ca^{2+}-dependent increase in its Ca^{2+} permeability (Bathori et al., 2006). However, enhancing the OMM permeability by tBid addition (Csordas et al., 2002) or overexpression of VDAC (Rapizzi et al., 2002) increased the IP3R-derived $[Ca^{2+}]_m$ signal in a relatively small extent compared to the amplification observed here.

The final barrier for Ca^{2+} to enter the mitochondrial matrix is the IMM, where mtCU has been established as a low-affinity highly selective Ca^{2+} channel (Kirichok et al., 2004). Complex, allosteric regulation and supralinear $[Ca^{2+}]_c$ activation of the mtCU has been described in earlier works on isolated mitochondria (Vinogradov and Scarpa, 1973; Kroner, 1986; Kirichok et al., 2004; Nicholls, 2005). Similarly, in permeabilized HeLa and RBL-2H3 cells we observed a progressive supralinear correlation between $[Ca^{2+}]_c$ (from ~0.7 to 30 μM) and the mitochondrial Ca^{2+} clearance rates (Csordas et al., 2013 and not shown, respectively). Thus, based on its activation properties, the mtCU could fit as a Ca^{2+} input-dependent amplifier in the process of local Ca^{2+} delivery from IP3R to the mitochondria. The mtCU is a protein complex of the pore forming subunit MCU (Baughman et al., 2011; De Stefani et al., 2011), transmembrane scaffold EMRE and regulatory Ca^{2+}-sensing EF-hand subunits MICU1 (Perocchi et al., 2010) and MICU2 (Plovanich et al., 2013) in the intermembrane space (Csordas et al., 2013; Sancak et al., 2013; Patron et al., 2014; Wang et al., 2014). MICU1 has dual role in mtCU activation: it is required to maintain a $[Ca^{2+}]_c$ threshold at low $[Ca^{2+}]_c$ levels (Mallilankaraman et al., 2012; Csordas et al., 2013) and to promote cooperativity at high $[Ca^{2+}]_c$ levels (Csordas et al., 2013; Logan et al., 2014; Patron et al., 2014). To promote cooperativity the EF hands of MICU1 seem to be required (Csordas et al., 2013). Overexpression of the MICU1ΔEF1,2 in the RBL-2H3 cells in this study brought about decreased cooperativity in the mtCU activation by SOCE as it was evidenced by the 50% decrease in the rate constant of the exponential rising phase of the $[Ca^{2+}]_m$ versus $[Ca^{2+}]_c$ plots (Figure 8). Thus, the mtCU, more specifically MICU1, likely functions as a supralinear signal amplifier that is robust enough to account for the Ca^{2+}_{ER}-dependent enhancement of IP3R-to-mitochondria local Ca^{2+} transfer.

Limitations

In several experiments, we used compartmentalized fura2-FF to measure $[Ca^{2+}]_m$. Although the compartmentalization of Ca^{2+} sensing dyes might be broad in many cell types, we have shown in several publications that in RBL-2H3 cells, under the cell culture and dye loading conditions used here, the vast majority of fura2-FF is confined to the mitochondria (Csordas et al., 1999; Csordas and Hajnoczky, 2001; Csordas and Hajnoczky, 2003; Csordas et al., 2006) Furthermore, when cells were permeabilized, cytoplasmic fura2-FF was washed out. Thus, fura2-FF is a validated indicator for

$[Ca^{2+}]_m$ in RBL-2H3 cells. Importantly, in intact cells, we measured $[Ca^{2+}]_m$ with both dye and genetically targeted reporters. Fura-2FF loaded to the mitochondrial matrix necessarily adds to the buffering, potentially altering the observed relationships between ER Ca^{2+} release and mitochondrial Ca^{2+} uptake and $[Ca^{2+}]_m$. However, the plateau level (~4 µM) is likely a feature of endogenous buffering as this is near the K_d of fura-2FF (4.5 µM) where additional Ca^{2+} binding by the dye is most sensitively reflected in fluorescence.

In many recent studies of ER Ca^{2+} handling, $[Ca^{2+}]$ in the ER lumen ($[Ca^{2+}]_{ER}$) was directly measured by Ca^{2+} sensitive fluorescent proteins targeted to the ER. To establish the quantitative relations among the amount of calcium stored in the ER, the IP_3-induced Ca^{2+} release, mitochondrial Ca^{2+} uptake and $[Ca^{2+}]_m$ we do not think that measurement of $[Ca^{2+}]_{ER}$ was needed. However, to link all these parameters to the $[Ca^{2+}]_{ER}$ levels, direct measurement of $[Ca^{2+}]_{ER}$ would be useful.

Even when the bulk Ca^{2+} release to the cytosol is a linear function of the ER Ca^{2+} load, the portion of the release exposing the mitochondria-ER interface (detected by the OMM-ER probe) may differ from other areas of the cell and potentially change with the ER loading. Because the increase of the $[Ca^{2+}]_{OMM\text{-}ER}$ peaks with the growing ER Ca^{2+} load could be approximated by a linear fit, we did not investigate further specific factors that might change with ER calcium loading and affect the $[Ca^{2+}]_{OMM\text{-}ER}$ signal spatial distribution.

Materials and Methods

Materials

IP_3 and Tg were purchased from Enzo Life Sciences or LC Laboratories Inc. (Woburn, MA); Ionomycin from Calbiochem (EMD Chemicals); Chelex 100 from BioRad (Hercules, CA). Fluorescent probes were from Teflabs (Austin, TX) except rhod-FF that was purchased from Molecular Probes/Invitrogen. All other chemicals were purchased from Fisher (Pittsburgh, PA) or Sigma (St. Louis, MO). Plasmid DNA encoding inverse and ratiometric pericams (Nagai et al., 2001) targeted to the mitochondrial matrix and m1 muscarinic receptor were a gift from Drs. Atsushi Miyawaki (RIKEN) and Tamás Balla (NIH), respectively. A low-affinity RCaMP developed by the Looger lab (Akerboom et al., 2013) was integrated into an mAKAP1-FKBP12-FP rapamycin-inducible OMM linker (Csordas et al., 2010). The cDNA for the double EF-hand mutant human MICU1 (Perocchi et al., 2010) was obtained from Addgene.

Live Cell Imaging

Delivery of genetically engineered $Ca^{2\pm}$ indicators. To measure $[Ca^{2+}]$ with fluorescent proteins, intact RBL-2H3 cells were transfected with cDNA encoding ratiometric or inverse pericam (targeted to mitochondrial matrix) or the rapamycin-inducible ER-OMM linker pair constructs mAKAP1(34-63)-FKBP12-RCaMPv (targeted to OMM, see below) plus CFP-FRB-9x-Sac1 (targeted to ER, Csordas et al., 2010) by means of electroporation in suspensions ($4.5{*}10^6$ cells + 10–20 µg of each cDNA in 300 µL medium). Electroporation was carried out in a BTX-830 square-pulse generator in a 4 mm gap cuvette using a single 250 V 13 ms pulse (Csordas et al., 2010).

Preparation of intact cells and loading of $Ca^{2\pm}$ indicator dyes. For microscopic imaging experiments, the cells were pre-incubated in a serum-free ECM (121 mM NaCl, 5 mM $NaHCO_3$, 10 mM Na-HEPES, 4.7 mM KCl, 1.2 mM KH_2PO_4, 1.2 mM $MgSO_4$, 2 mM $CaCl_2$, 10 mM glucose, pH7.4) containing 2% BSA and were loaded with fura-2/AM for measurements of $[Ca^{2+}]_c$ as described earlier (Csordas and Hajnoczky, 2003). After dye loading, the cells were washed into ECM with reduced BSA concentration (0.25%) and transferred to the microscope stage temperature controller (Warner Instruments) in an open (1 ml) teflon or surgical metal incubation chamber. For SOCE assays, $CaCl_2$ was omitted from the ECM and it was supplemented with the sarco-endoplasmic reticulum Ca^{2+} ATP-ase (SERCA) inhibitor Tg (2 µM).

Preparation of permeabilized cells, following pre-incubation in ECM w/2% BSA the cells were washed multiple times with a nominally Ca^{2+}-free extracellular salt solution containing 100 µM EGTA/Tris and transferred to the imaging chamber in 1 mL intracellular medium (ICM, composed of 120 mM KCl, 10 mM NaCl, 1 mM KH_2PO_4, and 20 mM Tris-HEPES at pH 7.2). Plasma membrane permeabilization was carried out using 25 µg/mL digitonin or 40 µg/mL saponin. After 5–7 min permeabilization period (35 °C), the cells were washed into fresh ICM supplemented with MgATP (2 mM) and succinate/Tris (2 mM).

Recording of $[Ca^{2+}]$ nanodomains at ER-mitochondrial associations was carried out as described previously (Csordas et al., 2010), except that the OMM-targeted Ca^{2+} sensor was an RCaMP (Yi et al., 2012). Briefly, we used a rapamycin-inducible ER-OMM linker system comprised of the FK506 binding protein (FKBP12) targeted to the OMM and tagged with RCaMPv, and the FKBP-rapamycin binding domain (FRB) of mTOR targeted to the ER and tagged by cyan fluorescent protein (CFP). Upon addition of rapamycin (100 nM during the 5 min permeabilization period) at the close ER-mitochondria interfaces where the FKBP and FRB domains are close enough to heterodimerize a crosslink between the organelles is established. Via lateral diffusion in the membranes the monomeric probes become recruited to these close interface areas in a couple of minutes where they get immobilized by the linkage. Further linkage formation that would expand the close SR-mitochondria interface was stopped by an FK506 (5 µM) wash. RCaMP fluorescence was normalized to the total Ca^{2+} sensitive range by the formula $F_{norm} = (F - F_{min})/(F_{max} - F_{min})$, where F_{max} and F_{min} were respectively determined at the end of the runs by sequential addition of a saturating (1 mM) $CaCl_2$ bolus (~300 μM free $[Ca^{2+}]$) and EGTA/Tris (pH 8.5) 10 mM. Based on its saturation curve the probe displayed relatively wide dynamic range, capable to resolve $[Ca^{2+}]$ changes between low 100 nMs up to 10 μM and reaching half-saturation at ~2 μM. Importantly, the relevant range used to establish correlation between Ca^{2+}_{ER} and IP3R-derived high $[Ca^{2+}]$ nanodomains ($[Ca^{2+}]_{OMM\text{-}ER}$ responses) fell between 15% and 60% probe saturation thus minimizing the chance that a sublinear correlation would arise from approaching saturation of the RCaMPv.

Fluorescence wide field imaging was carried out using a back-illuminated cooled CCD camera (PXL from Photometrics, 24 μm pixels) or an EM-CCD cameras (Hamamatsu ImagEM and Photometrics Evolve, respectively; both 512 × 512, 16 μm pixels), Uniblitz shutter and excitation filter wheel or a high-speed wavelength switcher (Lambda DG-4 from Sutter Instruments) fitted to either Olympus IX81 or IX70 inverted microscopes (40×, UApo340). For simultaneous $[Ca^{2+}]_c$ and $[Ca^{2+}]_m$, recording using fura-2 and inverse pericam, respectively 340/30, 380/20, and 490/20 nm excitation filters were used with a beam splitter 500 nm and emission filter 540/50 nm. The inverse pericam fluorescence at each time point was normalized to the initial fluorescence (F_0/F). When $[Ca^{2+}]_m$ was measured with ratiometric pericam 490/20 nm and 415/20 nm excitation filters and a 500 nm long-pass beam splitter were used. RCaMP fluorescence was excited through a 577/25 nm filter and detected through a dual band emission filter (Chroma 59022m: 523/27 and 634/39 nm) that allowed simultaneous recording with fura-2. To translate fura-2 ratio to molar $[Ca^{2+}]$ values in the intact cells, an in vitro calibration was performed as described in Bartok et al. (2019).

Fluorometry

Measurements of $[Ca^{2+}]_c$ and $[Ca^{2+}]_m$ in suspensions of permeabilized cells (approx. 2.4 mg protein/1.8 mL) were carried out as described earlier. We have demonstrated in previous studies that the compartmentalized fura-2FF (loaded in its acetoxymethylester/AM form) distributes in the mitochondrial matrix of RBL-2H3 cells (Csordas et al., 1999; Csordas and Hajnoczky, 2001).

Calibration of the $[Ca^{2\pm}]_c$. Changes with known Ca^{2+} amounts (0.5–2 μM $CaCl_2$→0.9–3.6 nmol Ca^{2+} pulses) in suspension of RBL-2H3 cells were carried out in the presence of mitochondrial uncoupler (FCCP 2 μM and oligomycin 5 μg/mL) and Tg (2 μM) to avoid active Ca^{2+} compartmentalization. When the range of $[Ca^{2+}]_c$ reached > 3 μM, it was monitored using fura-2FF (1 μM dye, K_d~4.5 μM) or rhodFF (0.5 μM dye, K_d~ 19 μM), in their water-soluble K^+-salt form, instead of rhod2 (K_d~1 μM). The calibration curve was established after correction to the $[Ca^{2+}]_c$ baseline shift caused by the SERCA inhibition from the beginning of the recording.

Statistics

All fluorometric recordings represent the mean response of approx. 10^7 cells and every recording was done at least in duplicates using the same cell preparation. Cumulative data are shown as mean ± SE, $n \geq 3$ cell preparations unless otherwise specified. Significance of differences from the relevant controls was calculated by Student's *t*-tests.

Acknowledgments

This work was supported by an NIH grants DK051526, DK125897, and HL142271 for GH, HL142864 for GC, and NKFI K134357 for VP.

Declaration of Conflicting Interests

The authors declared no potential conflicts of interest with respect to the research, authorship, and/or publication of this article.

Funding

The authors disclosed receipt of the following financial support for the research, authorship, and/or publication of this article: This work was supported by the National Heart, Lung, and Blood Institute, National Institute of Diabetes and Digestive and Kidney Diseases (grant numbers HL142271, DK051526, DK125897 for GH, HL142864 for GC, and NKFI K134357 for VP).

ORCID iD

György Hajnóczky https://orcid.org/0000-0002-1864-7510

References

Akerboom J, Carreras Calderon N, Tian L, Wabnig S, Prigge M, Tolo J, Gordus A, Orger MB, Severi KE, Macklin JJ, et al. (2013). Genetically encoded calcium indicators for multi-color neural activity imaging and combination with optogenetics. Front Mol Neurosci *6*, 2. doi: 10.3389/fnmol.2013.00002.

Bartok A, Weaver D, Golenar T, Nichtova Z, Katona M, Bansaghi S, Alzayady KJ, Thomas VK, Ando H, Mikoshiba K, et al. (2019). IP3 receptor isoforms differently regulate ER-mitochondrial contacts and local calcium transfer. Nat Commun *10*, 3726. doi: 10.1038/s41467-019-11646-3.

Bathori G, Csordas G, Garcia-Perez C, Davies E, Hajnoczky G (2006). Ca2+-dependent control of the permeability properties of the mitochondrial outer membrane and voltage-dependent anion-selective channel (VDAC). J Biol Chem *281*, 17347–17358.

Baughman JM, Perocchi F, Girgis HS, Plovanich M, Belcher-Timme CA, Sancak Y, Bao XR, Strittmatter L, Goldberger O, Bogorad RL, et al. (2011). Integrative genomics identifies MCU as an essential component of the mitochondrial calcium uniporter. Nature *476*, 341–345. doi: 10.1038/nature10234.

Bazil JN, Blomeyer CA, Pradhan RK, Camara AK, Dash RK (2013). Modeling the calcium sequestration system in isolated guinea pig cardiac mitochondria. J Bioenerg Biomembr *45*, 177–188. doi: 10.1007/s10863-012-9488-2.

Bernardi P (2013). The mitochondrial permeability transition pore: a mystery solved? Frontiers in physiology *4*, 95. doi: 10.3389/fphys.2013.00095.

Booth DM, Enyedi B, Geiszt M, Varnai P, Hajnoczky G (2016). Redox Nanodomains Are Induced by and Control Calcium Signaling at the ER-Mitochondrial Interface. Mol Cell *63*, 240–248. doi: 10.1016/j.molcel.2016.05.040.

Booth DM, Varnai P, Joseph SK, Hajnoczky G (2021). Oxidative bursts of single mitochondria mediate retrograde signaling toward the ER. Mol Cell *81*, 3866–3876 e3862. doi: 10.1016/j.molcel.2021.07.014.

Chalmers S, Nicholls DG (2003). The relationship between free and total calcium concentrations in the matrix of liver and brain mitochondria. J Biol Chem *278*, 19062–19070.

Csordas G, Golenar T, Seifert EL, Kamer KJ, Sancak Y, Perocchi F, Moffat C, Weaver D, de la Fuente Perez S, Bogorad R, et al. (2013). MICU1 controls both the threshold and cooperative activation of the mitochondrial Ca(2)(+) uniporter. Cell Metab *17*, 976–987. doi: 10.1016/j.cmet.2013.04.020.

Csordas G, Hajnoczky G (2001). Sorting of calcium signals at the junctions of endoplasmic reticulum and mitochondria. Cell Calcium *29*, 249–262.

Csordas G, Hajnoczky G (2003). Plasticity of mitochondrial calcium signaling. J Biol Chem *278*, 42273–42282.

Csordas G, Madesh M, Antonsson B, Hajnoczky G (2002). tcBid promotes Ca(2+) signal propagation to the mitochondria: control of Ca(2+) permeation through the outer mitochondrial membrane. Embo J *21*, 2198–2206.

Csordas G, Renken C, Varnai P, Walter L, Weaver D, Buttle KF, Balla T, Mannella CA, Hajnoczky G (2006). Structural and functional features and significance of the physical linkage between ER and mitochondria. J Cell Biol *174*, 915–921.

Csordas G, Thomas AP, Hajnoczky G (1999). Quasi-synaptic calcium signal transmission between endoplasmic reticulum and mitochondria. Embo J *18*, 96–108.

Csordas G, Varnai P, Golenar T, Roy S, Purkins G, Schneider TG, Balla T, Hajnoczky G (2010). Imaging interorganelle contacts and local calcium dynamics at the ER-mitochondrial interface. Mol Cell *39*, 121–132. doi: 10.1016/j.molcel.2010.06.029.

Csordas G, Weaver D, Hajnoczky G (2018). Endoplasmic Reticulum-Mitochondrial Contactology: Structure and Signaling Functions. Trends Cell Biol *28*, 523–540. doi: 10.1016/j.tcb.2018.02.009.

David G (1999). Mitochondrial clearance of cytosolic Ca(2+) in stimulated lizard motor nerve terminals proceeds without progressive elevation of mitochondrial matrix [Ca(2+)]. J Neurosci *19*, 7495–7506.

David G, Talbot J, Barrett EF (2003). Quantitative estimate of mitochondrial [Ca2+] in stimulated motor nerve terminals. Cell Calcium *33*, 197–206. doi: 10.1016/s0143-4160(02)00229-4.

de Brito OM, Scorrano L (2008). Mitofusin 2 tethers endoplasmic reticulum to mitochondria. Nature *456*, 605–610.

de la Fuente S, Fonteriz RI, de la Cruz PJ, Montero M, Alvarez J (2012). Mitochondrial free [Ca(2+)] dynamics measured with a novel low-Ca(2+) affinity aequorin probe. Biochem J *445*, 371–376. doi: 10.1042/BJ20120423.

De Stefani D, Raffaello A, Teardo E, Szabo I, Rizzuto R (2011). A forty-kilodalton protein of the inner membrane is the mitochondrial calcium uniporter. Nature *476*, 336–340. doi: 10.1038/nature10230.

Denton RM, McCormack JG (1986). The calcium sensitive dehydrogenases of vertebrate mitochondria. Cell Calcium *7*, 377–386.

Denton RM, McCormack JG, Edgell NJ (1980). Role of calcium ions in the regulation of intramitochondrial metabolism. Effects of Na+, Mg2 + and ruthenium red on the Ca2+-stimulated oxidation of oxoglutarate and on pyruvate dehydrogenase activity in intact rat heart mitochondria. Biochem J *190*, 107–117.

Foyouzi-Youssefi R, Arnaudeau S, Borner C, Kelley WL, Tschopp J, Lew DP, Demaurex N, Krause KH (2000). Bcl-2 decreases the free Ca2 + concentration within the endoplasmic reticulum. Proceedings of the National Academy of Sciences of the United States of America *97*, 5723–5728.

Giacomello M, Drago I, Bortolozzi M, Scorzeto M, Gianelle A, Pizzo P, Pozzan T (2010). Ca2 + hot spots on the mitochondrial surface are generated by Ca2 + mobilization from stores, but not by activation of store-operated Ca2 + channels. Mol Cell *38*, 280–290.

Gunter TE, Pfeiffer DR (1990). Mechanisms by which mitochondria transport calcium. Am J Physiol *258*, C755–786.

Hajnoczky G, Hager R, Thomas AP (1999). Mitochondria suppress local feedback activation of inositol 1,4, 5-trisphosphate receptors by Ca2 + . J Biol Chem *274*, 14157–14162.

Hajnoczky G, Robb-Gaspers LD, Seitz MB, Thomas AP (1995). Decoding of cytosolic calcium oscillations in the mitochondria. Cell *82*, 415–424.

Hajnoczky G, Thomas AP (1994). The inositol trisphosphate calcium channel is inactivated by inositol trisphosphate. Nature *370*, 474–477. doi: 10.1038/370474a0.

Hansford RG (1987). Relation between cytosolic free Ca2 + concentration and the control of pyruvate dehydrogenase in isolated cardiac myocytes. Biochem J *241*, 145–151.

Hayashi T, Su TP (2007). Sigma-1 receptor chaperones at the ER-mitochondrion interface regulate Ca(2+) signaling and cell survival. Cell *131*, 596–610. doi: 10.1016/j.cell.2007.08.036.

Horne JH, Meyer T (1995). Luminal calcium regulates the inositol trisphosphate receptor of rat basophilic leukemia cells at a cytosolic site. Biochemistry *34*, 12738–12746.

Hoth M, Fanger CM, Lewis RS (1997). Mitochondrial regulation of store-operated calcium signaling in T lymphocytes. J Cell Biol *137*, 633–648.

Jouaville LS, Ichas F, Holmuhamedov EL, Camacho P, Lechleiter JD (1995). Synchronization of calcium waves by mitochondrial substrates in Xenopus laevis oocytes. Nature *377*, 438–441. doi: 10.1038/377438a0.

Jouaville LS, Pinton P, Bastianutto C, Rutter GA, Rizzuto R (1999). Regulation of mitochondrial ATP synthesis by calcium: evidence for a long-term metabolic priming. Proc Natl Acad Sci U S A *96*, 13807–13812.

Katona M, Bartok A, Nichtova Z, Csordas G, Berezhnaya E, Weaver D, Ghosh A, Varnai P, Yule DI, Hajnoczky G (2022). Capture at the ER-mitochondrial contacts licenses IP(3) receptors to stimulate local Ca(2+) transfer and oxidative metabolism. Nat Commun *13*, 6779. doi: 10.1038/s41467-022-34365-8.

Kirichok Y, Krapivinsky G, Clapham DE (2004). The mitochondrial calcium uniporter is a highly selective ion channel. Nature *427*, 360–364.

Kroner H (1986). Ca2 + ions, an allosteric activator of calcium uptake in rat liver mitochondria. Arch Biochem Biophys *251*, 525–535.

Lin X, Varnai P, Csordas G, Balla A, Nagai T, Miyawaki A, Balla T, Hajnoczky G (2005). Control of calcium signal propagation to the mitochondria by inositol 1,4,5-trisphosphate-binding proteins. J Biol Chem *280*, 12820–12832. doi: 10.1074/jbc.M411591200.

Logan CV, Szabadkai G, Sharpe JA, Parry DA, Torelli S, Childs AM, Kriek M, Phadke R, Johnson CA, Roberts NY, et al. (2014). Loss-of-function mutations in MICU1 cause a brain and muscle disorder linked to primary alterations in mitochondrial calcium signaling. Nat Genet *46*, 188–193. doi: 10.1038/ng.2851.

Ma TS, Mann DL, Lee JH, Gallinghouse GJ (1999). SR compartment calcium and cell apoptosis in SERCA overexpression. Cell Calcium *26*, 25–36.

Malli R, Frieden M, Osibow K, Zoratti C, Mayer M, Demaurex N, Graier WF (2003). Sustained Ca2 + transfer across mitochondria is Essential for mitochondrial Ca2 + buffering, sore-operated Ca2 + entry, and Ca2 + store refilling. J Biol Chem *278*, 44769–44779.

Mallilankaraman K, Doonan P, Cardenas C, Chandramoorthy HC, Muller M, Miller R, Hoffman NE, Gandhirajan RK, Molgo J, Birnbaum MJ, et al. (2012). MICU1 is an essential gatekeeper for MCU-mediated mitochondrial Ca(2+) uptake that regulates cell survival. Cell *151*, 630–644. doi: 10.1016/j.cell.2012.10.011.

Marchant JS, Ramos V, Parker I (2002). Structural and functional relationships between Ca2 + puffs and mitochondria in Xenopus oocytes. American journal of physiology. Cell physiology *282*, C1374–1386. doi: 10.1152/ajpcell.00446.2001.

Mendes CC, Gomes DA, Thompson M, Souto NC, Goes TS, Goes AM, Rodrigues MA, Gomez MV, Nathanson MH, Leite MF (2005). The type III inositol 1,4,5-trisphosphate receptor preferentially transmits apoptotic Ca2 + signals into mitochondria. J Biol Chem *280*, 40892–40900. doi: 10.1074/jbc.M506623200.

Missiaen L, De Smedt H, Droogmans G, Casteels R (1992). Ca2 + release induced by inositol 1,4,5-trisphosphate is a steady-state phenomenon controlled by luminal Ca2 + in permeabilized cells. Nature *357*, 599–602.

Montero M, Alonso MT, Carnicero E, Cuchillo-Ibanez I, Albillos A, Garcia AG, Garcia-Sancho J, Alvarez J (2000). Chromaffin-cell stimulation triggers fast millimolar mitochondrial Ca2 + transients that modulate secretion. Nat Cell Biol *2*, 57–61.

Nagai T, Sawano A, Park ES, Miyawaki A (2001). Circularly permuted green fluorescent proteins engineered to sense Ca2 + . Proc Natl Acad Sci U S A *98*, 3197–3202.

Nicholls DG (2005). Mitochondria and calcium signaling. Cell Calcium *38*, 311–317.

Nicholls DG, Chalmers S (2004). The integration of mitochondrial calcium transport and storage. J Bioenerg Biomembr *36*, 277–281.

Oldershaw KA, Taylor CW (1993). Luminal Ca2 + increases the affinity of inositol 1,4,5-trisphosphate for its receptor. Biochem J *292*(Pt 3), 631–633.

Olson ML, Chalmers S, McCarron JG (2010). Mitochondrial Ca2 + uptake increases Ca2 + release from inositol 1,4,5-trisphosphate receptor clusters in smooth muscle cells. J Biol Chem *285*, 2040–2050. doi: 10.1074/jbc.M109.027094.

Pacher P, Csordas P, Schneider T, Hajnoczky G (2000). Quantification of calcium signal transmission from sarco-endoplasmic reticulum to the mitochondria. J Physiol *529*(Pt 3), 553–564.

Pacher P, Sharma K, Csordas G, Zhu Y, Hajnoczky G (2008). Uncoupling of ER-mitochondrial calcium communication by transforming growth factor-beta. Am J Physiol Renal Physiol *295*, F1303–1312.

Patron M, Checchetto V, Raffaello A, Teardo E, Vecellio Reane D, Mantoan M, Granatiero V, Szabo I, De Stefani D, Rizzuto R (2014). MICU1 and MICU2 finely tune the mitochondrial Ca2 + uniporter by exerting opposite effects on MCU activity. Molecular cell *53*, 726–737. doi: 10.1016/j.molcel.2014.01.013.

Perocchi F, Gohil VM, Girgis HS, Bao XR, McCombs JE, Palmer AE, Mootha VK (2010). MICU1 encodes a mitochondrial EF hand protein required for Ca(2+) uptake. Nature *467*, 291–296.

Pinton P, Ferrari D, Magalhaes P, Schulze-Osthoff K, Di Virgilio F, Pozzan T, Rizzuto R (2000). Reduced loading of intracellular Ca(2+) stores and downregulation of capacitative Ca(2+) influx in Bcl-2-overexpressing cells. J Cell Biol *148*, 857–862.

Pinton P, Ferrari D, Rapizzi E, Di Virgilio F, Pozzan T, Rizzuto R (2001). The Ca2 + concentration of the endoplasmic reticulum is a key determinant of ceramide-induced apoptosis: significance for the molecular mechanism of Bcl-2 action. Embo J *20*, 2690–2701.

Pinton P, Giorgi C, Siviero R, Zecchini E, Rizzuto R (2008). Calcium and apoptosis: ER-mitochondria Ca2 + transfer in the control of apoptosis. Oncogene *27*, 6407–6418.

Plovanich M, Bogorad RL, Sancak Y, Kamer KJ, Strittmatter L, Li AA, Girgis HS, Kuchimanchi S, De Groot J, Speciner L, et al. (2013). MICU2, a paralog of MICU1, resides within the mitochondrial uniporter complex to regulate calcium handling. PLoS One *8*, e55785. doi: 10.1371/journal.pone.0055785.

Rapizzi E, Pinton P, Szabadkai G, Wieckowski MR, Vandecasteele G, Baird G, Tuft RA, Fogarty KE, Rizzuto R (2002). Recombinant expression of the voltage-dependent anion channel enhances the transfer of Ca2 + microdomains to mitochondria. J Cell Biol *159*, 613–624.

Rizzuto R, Pinton P, Carrington W, Fay FS, Fogarty KE, Lifshitz LM, Tuft RA, Pozzan T (1998). Close contacts with the endoplasmic reticulum as determinants of mitochondrial Ca2 + responses. Science *280*, 1763–1766.

Rizzuto R, Simpson AW, Brini M, Pozzan T (1992). Rapid changes of mitochondrial Ca2 + revealed by specifically targeted recombinant aequorin. Nature *358*, 325–327.

Robb-Gaspers LD, Burnett P, Rutter GA, Denton RM, Rizzuto R, Thomas AP (1998). Integrating cytosolic calcium signals into mitochondrial metabolic responses. Embo J *17*, 4987–5000.

Sancak Y, Markhard AL, Kitami T, Kovacs-Bogdan E, Kamer KJ, Udeshi ND, Carr SA, Chaudhuri D, Clapham DE, Li AA, et al. (2013). EMRE is an essential component of the mitochondrial calcium uniporter complex. Science *342*, 1379–1382. doi: 10.1126/science.1242993.

Scorrano L, De Matteis MA, Emr S, Giordano F, Hajnoczky G, Kornmann B, Lackner LL, Levine TP, Pellegrini L, Reinisch K, et al. (2019). Coming together to define membrane contact sites. Nat Commun *10*, 1287. doi: 10.1038/s41467-019-09253-3.

Scorrano L, Oakes SA, Opferman JT, Cheng EH, Sorcinelli MD, Pozzan T, Korsmeyer SJ (2003). BAX and BAK regulation of endoplasmic reticulum Ca2+: a control point for apoptosis. Science *300*, 135–139.

Spat A, Szanda G, Csordas G, Hajnoczky G (2008). High- and low-calcium-dependent mechanisms of mitochondrial calcium signalling. Cell Calcium *44*, 51–63.

Suzuki J, Kanemaru K, Ishii K, Ohkura M, Okubo Y, Iino M (2014). Imaging intraorganellar Ca2 + at subcellular resolution using CEPIA. Nat Commun *5*, 4153. doi: 10.1038/ncomms 5153.

Szabadkai G, Bianchi K, Varnai P, De Stefani D, Wieckowski MR, Cavagna D, Nagy AI, Balla T, Rizzuto R (2006). Chaperone-mediated coupling of endoplasmic reticulum and mitochondrial Ca2 + channels. J Cell Biol *175*, 901–911.

Szabadkai G, Duchen MR (2008). Mitochondria: the hub of cellular Ca2 + signaling. Physiology (Bethesda *23*, 84–94.

Szalai G, Krishnamurthy R, Hajnoczky G (1999). Apoptosis driven by IP(3)-linked mitochondrial calcium signals. Embo J *18*, 6349–6361.

Tinel H, Cancela JM, Mogami H, Gerasimenko JV, Gerasimenko OV, Tepikin AV, Petersen OH (1999). Active mitochondria surrounding the pancreatic acinar granule region prevent spreading of inositol trisphosphate-evoked local cytosolic Ca(2+) signals. Embo J *18*, 4999–5008.

Tosatto A, Rizzuto R, Mammucari C (2017). Ca(2+) Measurements in Mammalian Cells with Aequorin-based Probes. Bio Protoc *7*. doi: 10.21769/BioProtoc.2155.

Vais H, Foskett JK, Ullah G, Pearson JE, Mak DO (2012). Permeant calcium ion feed-through regulation of single inositol 1,4,5-trisphosphate receptor channel gating. J Gen Physiol *140*, 697–716. doi: 10.1085/jgp.201210804.

Vais H, Wang M, Mallilankaraman K, Payne R, McKennan C, Lock JT, Spruce LA, Fiest C, Chan MY, Parker I, et al. (2020). ER-luminal [Ca(2+)] regulation of InsP(3) receptor gating mediated by an ER-luminal peripheral Ca(2+)-binding protein. Elife *9*, e53531. doi: 10.7554/eLife.5353153531.

Vinogradov A, Scarpa A (1973). The initial velocities of calcium uptake by rat liver mitochondria. J Biol Chem *248*, 5527–5531.

Wang L, Yang X, Li S, Wang Z, Liu Y, Feng J, Zhu Y, Shen Y (2014). Structural and mechanistic insights into MICU1 regulation of mitochondrial calcium uptake. EMBO J *33*, 594–604. doi: 10.1002/embj.201386523.

Wei AC, Liu T, Winslow RL, O'Rourke B (2012). Dynamics of matrix-free Ca2 + in cardiac mitochondria: two components of Ca2 + uptake and role of phosphate buffering. J Gen Physiol *139*, 465–478. doi: 10.1085/jgp.201210784.

Wilson BS, Pfeiffer JR, Smith AJ, Oliver JM, Oberdorf JA, Wojcikiewicz RJ (1998). Calcium-dependent clustering of inositol 1,4,5-trisphosphate receptors. Mol Biol Cell *9*, 1465–1478.

Yi M, Weaver D, Eisner V, Varnai P, Hunyady L, Ma J, Csordas G, Hajnoczky G (2012). Switch from ER-mitochondrial to SR-mitochondrial calcium coupling during muscle differentiation. Cell Calcium *52*, 355–365. doi: 10.1016/j.ceca.2012.05.012.

Yi M, Weaver D, Hajnoczky G (2004). Control of mitochondrial motility and distribution by the calcium signal: a homeostatic circuit. J Cell Biol *167*, 661–672.